Applied Energy 314 (2022) 118881

Contents lists available at ScienceDirect

Applied Energy

journal homepage: www.elsevier.com/locate/apenergy

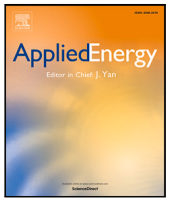

A methodology for an optimal design of ground-mounted photovoltaic power plants

A. Barbón [a], C. Bayón-Cueli [c], L. Bayón [b,*], V. Carreira-Fontao [c]

[a] Department of Electrical Engineering, University of Oviedo, Spain
[b] Department of Mathematics, University of Oviedo, Spain
[c] Polytechnic School of Engineering of Gijón, University of Oviedo, Spain

ARTICLE INFO

Keywords:
Ground-mounted photovoltaic power plant
Packing algorithm
Rack configuration
Structural analysis
Cost analysis

ABSTRACT

A methodology for estimating the optimal distribution of photovoltaic modules with a fixed tilt angle in ground-mounted photovoltaic power plants has been described. It uses Geographic Information System, available in the public domain, to estimate Universal Transverse Mercator coordinates of the area which has been selected for the installation of the photovoltaic plant. An open-source geographic information system software, *QGIS*, has been used. The estimation of the solar irradiance takes into account the variations in the local cloud cover distribution. The optimization process is considered to maximize the amount of energy absorbed by the photovoltaic plant using a packing algorithm (in Mathematica™ software). This packing algorithm calculates the shading between photovoltaic modules. This methodology can be applied to any photovoltaic plant. Different rack configurations and tilt angles are incorporated in the study to account for the characteristics of the irregular shape of the land. The most used rack configurations in photovoltaic plants are the $2V \times 12$ configuration (2 vertically modules in each row and 12 modules per row) and the $3V \times 8$ configuration (3 vertically consecutive modules in each row and 8 modules per row). Codes and standards have been used for the structural analysis of these rack configurations. For this purpose, the wind loads, the snow loads, the weight of the structure, the weight of the photovoltaic modules, and combinations thereof have been calculated. This analysis has been performed with AutoDesk Robot Structural Analysis software for the different rack configurations. A detailed cost analysis of the most used rack configurations in photovoltaic plants has been presented. The levelized cost of the produced electricity efficiency is calculated for each rack configuration. The methodology has been applied in Sigena I photovoltaic plant located in Northeast of Spain. The current rack configuration used in this photovoltaic plant is the $2V \times 12$ configuration with a tilt angle of 30 (°). The configurations $3V \times 8$ configuration with a tilt angle of 14 (°) and $2V \times 12$ configuration with a tilt angle of 22 (°) are the best options proposed by the optimization algorithm. The results show that the $3V \times 8$ configuration with a tilt angle of 14 (°) increases the amount of energy captured by up to 32.45% in relation to the current configuration of Sigena I photovoltaic plant with a levelized cost of the produced electricity efficiency of 1.10. In the other hand, the $3V \times 8$ configuration increases the amount of energy captured by up to 19.52% in relation to the $2V \times 12$ configuration with a tilt angle of 22 (°) with a levelized cost of the produced electricity efficiency of 1.05. The $3V \times 8$ configuration is the one which has the lowest cost for the same number of photovoltaic modules. The $2V \times 12$ configuration with a tilt angle of 30 (°) increases the cost by up to 32.48% in relation to a $3V \times 8$ configuration with a tilt angle of 14 (°).

1. Introduction

The goals of the Paris Agreement [1] have shown the way to reduce the environmental impact caused by the use of fossil fuels and to replace them by renewable energy resources. Concerned by these agreements, many countries have set ambitious plans to introduce renewable energy resources [2]. Particularly, the use of the solar energy has continuously increased during the last decade [3]. Photovoltaic (PV) systems and concentrated solar power are two solar energy applications to produce electricity on a large-scale.

The photovoltaic technology is an evolved technology of renewable energy which is rapidly spreading due to a different factors such as: (i) Its continuous decrease in the costs of the system components. The

* Corresponding author.
E-mail address: bayon@uniovi.es (L. Bayón).

https://doi.org/10.1016/j.apenergy.2022.118881
Received 15 November 2021; Received in revised form 20 January 2022; Accepted 12 February 2022
Available online 22 March 2022

Nomenclature

A_{PV}	Photovoltaic module area (m^2)
A_{PVeff}	Effective PV modules area(m^2)
A_{TPV}	Total photovoltaic modules area (m^2)
B	Length of the shadow (m)
C_{cb}	Costs of the cable (€)
C_e	Exposure factor
C_i	Initial investment cost (€)
C_{inv}	Unit cost of the inverter (€/unit)
C_L	Cost of the land area (€)
C_M	Costs of the monitoring system (€)
C_{MS}	Unit cost of the mounting structure (€/unit)
C_{OM}	Cost of operation and maintenance (€)
C_p	Pressure coefficient
C_{pd}	Costs of the protection devices (€)
C_{prob}	Probability factor
C_{PV}	Unit cost of a PV module (€/unit)
C_T	Costs of the transformer (€)
d	Annual degradation rate
EG	Energy gain (%)
E_a	Annual energy (MWh)
E_i	Total electrical energy output at the ith year (kWh)
E_{PV}	Total energy on the photovoltaic modules (MWh)
e_l	Longitudinal distance (m)
e_l^m	Longitudinal maintenance distance (m)
e_l^{st}	Longitudinal standard distance (m)
e_t	Transversal installation distance (m)
$\mathbb{H}_t$	Adjusted total irradiation on a tilted surface (Wh/m^2)
k	Parameter that depend on the terrain
I	Lifetime of the project ($years$)
$\mathbb{I}_{bh}$	Adjusted beam irradiance on a horizontal surface (W/m^2)
$\mathbb{I}_{dh}$	Adjusted diffuse irradiance on a horizontal surface (W/m^2)
$\mathbb{I}_h$	Adjusted total irradiance on a horizontal surface (W/m^2)
L	Length of the rack configuration (m)
L_e	Parameter that depend on the terrain
L_{PV}	Length of the photovoltaic modules (m)
$LCOE$ efficiency	Ratio between the $LCOEs$ rack configurations
N_{inv}	Total number of inverters
N_{MS}	Total number of mounting structures
N_{PV}	Number of photovoltaic modules
n	Ordinal of the day (day)
np	Maximum number of photovoltaic modules
$npss$	Number of photovoltaic modules unaffected by shadows
$\overline{P}$	Available land area (m^2)
q_b	Basic velocity pressure (kN/m^2)
q_e	Static pressure (kN/m^2)
q_{PV}	Load due to the weight of the PV modules (kN/m^2)
r	Discount rate for ith year
S	Projection the L on the horizontal plane (m)
S_i	Availability of solar resource at the ith year (kWh)
S_L	Snow load (kg)
T	Solar time (h)
T_R	Sunrise solar time (h)
T_S	Sunset solar time (h)
T_1, T_2	Operating hours of the PV system (h)
v_b	Basic wind velocity (m/s)
W	Width of the rack configuration (m)
W_{ePV}	Weight of the PV module (kg)
W_{eS}	Weight of the structure (kg)
W_L	Wind load (kg)
W_{PV}	Width of the photovoltaic modules (m)
z	Height on the ground (m)
α_S	Height angle of the Sun (°)
β	Tilt angle of photovoltaic module (°)
β^*	Tilt angle of photovoltaic module for the maximization of the total energy(°)
γ	Azimuth angle of photovoltaic module (°)
γ_S	Azimuth of the Sun (°)
δ	Solar declination (°)
η	Performance factor
θ_i	Incidence angle (°)
θ_l	Longitudinal incidence angle (°)
θ_{l0}	Longitudinal incidence angle that minimizes shadowing effects (°)
θ_z	Zenith angle of the Sun (°)
λ	Latitude angle (°)
ρ	Air density (Kg/m^3)
ρ_g	Ground reflectance (dimensionless)
ω	Hour angle (°)

weighted average of the levelized cost of energy ($LCOE$) in 2018 was 0.085 (USD/kWh), and it is forecasted to be between 0.02 and 0.08 (USD/kWh) by 2030 and between 0.014 and 0.05 (USD/kWh) by 2050 [4]; (ii) Its versatility and modularity. There is a large quantity of commercial PV modules with different sizes and different power capacities which allow a photovoltaic installation to be adapted to any particular area; (iii) Its minimum maintenance cost. Despite the lack of standardization [5] for this value, the National Renewable Energy Laboratory recommends assuming an annual cost of 0.5% of the total initial cost for the large systems, and 1% for the small ones. Moreover, Mortensen [6] suggests that operation and maintenance costs of photovoltaics with tracking systems are double those of fixed-tilt ones; (iv) Its institutional economic support. The European Union (EU) countries provide incentives for newly created capacity of renewable energies [2]. This technology has also disadvantages: (i) It does not provide a continuous supply of energy, as it depends on solar irradiance; (ii) It needs an energy storage system to supply energy during the night; (iii) It is necessary to schedule the cleaning of the PV modules to maintain an optimum performance and avoid damage to modules.

Solar PV plants whose capacities range from 1 (MW) to 100 (MW) [7] are considered to be large-scale PV plants and they require a surface that exceeds 1 (km^2) [8]. A large-scale PV plant comprises: PV modules, mounting system, inverters, transformation centre, cables, electrical protection systems, measurement equipments and system monitoring. The PV modules produce electricity in direct current from

solar irradiance and the inverters convert this current into alternating current which can be injected into the electricity grid. The optimization of the design of large-scale PV plants is essential to reduce their high cost. Due to the high number of components required in the installation of PV plants, the optimization may have different approaches. Zidane et al. [9] have compared the technology of crystalline silicon to that of thin-film cadmium telluride to determine the suitable PV module for the large-scale PV plants. The optimization process is considered to minimize the $LCOE$. Bakhshi-Jafarabadi et al. [10] have proposed a new formulation to convert the problem of the PV plants design to a binary linear programming to optimize its economic design. Simola et al. [11] have studied the profitability of a PV plant in the conditions of southern Finland, with the simulation of a grocery store, a dairy farm and a domestic house with space heating by electric current. Şenol et al. [12] have proposed a methodology to optimize the design of a large-scale PV plant and a guide for investors and technical staff to the design of such a system, with emphasis on self-consumption policy. Sulaiman et al. [13] have proposed an intelligent sizing technique to design grid-connected PV systems considering different types of PV modules and inverters. Fernández-Infantes et al. [14] have presented a specific computer application for the optimizing the parameters of grid-connected PV plant (inverter size, losses due to electric conductors, etc.). However, these works have neglected the optimization of the distribution of PV modules.

The racking systems for PV modules used in large-scale PV plants can be classified into two types: racking systems with a fixed tilt angle and racking systems with a variable tilt angle. The first type, ground-mounted photovoltaic, has a fixed tilt angle for a fixed period of time. The second type uses a solar tracker system that follows Sun direction so that the maximum power is obtained. The solar tracking can be implemented with two axes of rotation (dual-axis trackers) or with a single axis of rotation (single-axis trackers). The single-axis trackers can have different orientations: horizontal North–South, horizontal East–West and parallel to the Earth's axis. In practice, the most used ones are aligned with the North–South direction. The dual-axis trackers increase the production compared to a ground-mounted photovoltaic (a gain from 12 up to 28% [15]), and they also increase the production compared to a single-axis tracker (a gain from 3 up to 16% [15]), depending on the location of the PV plant. Although the racking systems with a variable tilt angle produce a greatest total energy, it is needed to take into account other factors such as the initial investment cost, the costs of operation and maintenance, the topography, the available land area, the soil conditions, the wind loads, etc. A dual-axis tracker usually represents a 40–50% increase in the average installation costs over a system of the same size with fixed tilt angle and a 20−25% over a system of similar size with a single axis tracker [16]. On the other hand, the moving parts of the solar trackers reduce their expected lifetime and increase the operation and maintenance costs [16]. Another important aspect is the wind loads that affect the solar tracking systems to a greater extent.

Another aspect to be considered is the available land area. In a large-scale PV plant it is worth to distinguish between the total and the direct land area [17]. All the land enclosed by the site boundary is the total land area whereas the land area comprises the land occupied by: PV modules, buildings (office and sanitary rooms, low voltage/ medium voltage station, medium voltage/high voltage station, communications) and access roads. In this work, the land occupied by the PV modules will be analysed in more detail. The land occupied by the PV modules is the area of the PV generator, therefore it can be associated with the generated PV energy. Therefore, an analysis of this parameter is necessary during the design phase of a PV plant. However, there are few available studies in the literature about the area occupied by PV modules in PV plants. Researchers have focused their attention on the statistical study of the direct land area. Ong et al. [18] have presented an analysis of the land use associated with PV plants in the United States. This report shows the land use for various rack configurations.

Table 1
Advantages and disadvantages of mounting systems.

Parameter	Dual-axis tracker	Single-axis tracker	Ground-mounted photovoltaic
Energy production	Advantage	Advantage	Disadvantage
Initial investment cost	Disadvantage	Disadvantage	Advantage
Operation and maintenance cost	Disadvantage	Disadvantage	Advantage
Available land area	Advantage	Advantage	Disadvantage
Soil conditions	Disadvantage	Disadvantage	Advantage
Wind loads	Disadvantage	Disadvantage	Advantage

For example, for racking systems with a fixed tilt angle the direct land area is 2.22 to 2.34 (ha/MWac) and for racking systems with a single-axis tracker aligned with the North–South axis the direct land area is 2.54 to 3.64 (ha/MWac). Fthenakis et al. [17] have also presented a study about the land use associated with PV plants. In this study, the direct land area necessary for racking systems with a fixed tilt angle and for single-axis tracker aligned with the North–South axis is 2.20 (ha/MWac) and 2.50 (ha/MWac) respectively. On the other hand, Denholm and Margolis [8] have got lower values for both racking systems: 1.50 (ha/MWac) for systems with a fixed tilt angle and 2.10 (ha/MWac) for systems with a single-axis tracker aligned with the North–South axis.

Table 1 shows a summary of the advantages and disadvantages of each mounting system.

In order to estimate the area occupied by PV modules, some authors work with terms such as the packing factor [18,19], the ground cover ratio [19,20], the spacing factor [21] and the occupation factor [19,22]. The first two terms refer to the ratio between the area actually occupied by the PV modules and the total area necessary for installation of the PV modules. The other two terms refer to the inverse instead.

The selection of the most suitable locations for photovoltaic (PV) plants is a prior aim for the sector companies. Geographic information system (GIS) is a framework used for analysing the possibility of PV plants installation [23]. With GIS tools the potential of solar power and the suitable locations for PV plants can be estimated. This computer system has geographic constraints such as (e.g. latitude, slope). For instance, Lindberg et al. [24] have presented a methodology for a utility-scale solar guide by studying the hosting capacity in the local grid and identifying the appropriate land for PV parks. Zhang et al. [25] have evaluated the solar energy potential in China. For this purpose, they have examined the spatial–temporal distribution of solar energy resources from geographical, technological and economic points of view. Yang et al. [23], basing on a GIS-based model, have studied 600 land conversion factors to carefully estimate the generation potential for large-scale PV power generation in China.

A ground-mounted photovoltaic power plant comprises a large number of components such as: photovoltaic modules, mounting systems, inverters, power transformer. Therefore its optimization may have different approaches. In this paper, the mounting system with a fixed tilt angle has been studied. Once the racking system has been fixed, for the same available land and same type of PV module, the generated energy depends on variables such as the tilt angle of the PV module and the inter-row spacing, that is, the distribution of PV modules on the available land. To solve this problem is complex because large-scale PV plants are composed of several thousands of PV modules. The objective of this paper is to conduct an optimization of the distribution of PV modules in large-scale PV plants, based on the currently available geographic data and the solar irradiation data. The main outcomes will provide fundamental information to aid power companies in optimizing the deployment of large-scale PV plants across the countries worldwide. To realize this goal, this work is conducted with the following methodology: (i) To identify the geographical location of the project; (ii) To get the UTM (Universal Transverse Mercator) coordinates of the available land area; (iii) To convert the UTM coordinates into the $Mathematica$™software; (iv) To choose the rack configuration; (v) To

choose the objective function; (vi) To do a shadows study; (vii) To develop the optimization algorithm; (viii) To do a structural analysis of the mounting system and (ix) To analyse the costs.

This work is based on two previous studies, [26,27]. The first one is a more uncomplicated study which only takes into account rectangular shapes. The second one takes into account terraces with more general geometric shapes, but it imposes certain working conditions in order to guarantee the absence of shading between the modules. It generalizes the study from several points of view:

(i) The land can be any irregular shape given that this is the usual form of PV plants.
(ii) The size of land can be bigger than that of any building terrace.
(iii) The algorithm that is presented in this work maximizes the total energy of the PV modules of the PV plant for each tilt angle β, taking into account the shading between the rows of PV modules.

The specific contributions of this study can be summarized in the following proposals:

(i) A methodology to maximize the amount of energy absorbed by the PV plant.
(ii) The algorithm which is presented in this work for each tilt angle β, maximizes the total energy of the PV modules of the PV plant, taking into account the shading between the rows of PV modules.
(iii) A detailed analysis of the loads (wind loads, snow loads, weight of the structure, weight of the PV modules, and combinations thereof) on mounting systems with a fixed tilt angle.
(iv) A detailed analysis of the costs of mounting systems with a fixed tilt angle.

In the bullet (i), the essential part of the proposed methodology is intended to solve the classical packing mathematical problem. Furthermore, the proposed methodology helps answer a number of practical questions such as: how many PV modules can be installed?, which is the tilt angle of the PV modules? and which is the right position for the PV modules?

Another practical consideration is shown in bullet (ii), since the algorithm allows the choice of the tilt angle of the PV modules to obtain the number and position of the PV modules.

With regard to bullet (iii), it is important to evaluate the mounting systems in order to ensure that the PV modules will remain attached to their structures during windstorms and that additional loads or load concentrations do not exceed the structural capacity of the mounting system.

To assess the cost-effectiveness of a PV plant, it is necessary to know the cost of the chosen mounting system. This aspect is discussed in bullet (iv).

The optimum tilt angle for a single PV module, will never be the tilt angle that have been selected for the whole PV plant. In fact, as it will be demonstrated, the use of tilt angles with values close to the value of the place latitude, puts up the cost of the mounting system and does not increase the amount of energy absorbed by the PV plant. The research provides important information for the design of photovoltaic plants, from both the energy and the economic point of view.

The paper is structured as follows; In Section 2 shows the background and a model to estimate the solar irradiance. Section 3 outlines the methodology which is proposed. Section 4 presents the results obtained from the case that has been studied. Finally, Section 5 summarizes the main contributions and the conclusions of the paper itself.

2. Background

2.1. Suitable land for large-scale PV plants

Most solar technologies are installed in rural environments, where the landscape has remained almost unaltered. Therefore, land occupation of these installations may transform rural environments, although PV plants are the solar technology that less transforms and occupies the land [17]. The land assessment gives us the suitable areas for PV plants. Knowledge of the dimensions, altitude, shape and slope of the land are essential to evaluate the rack configuration for a particular PV installation project.

The shape of the land limits the design of a PV plant. A square shape of the land enables a good distribution of PV modules [26], but the majority of the large-scale PV plants are to be installed in irregular shape areas.

On the other hand, it is necessary to tackle each project in a particular way to adapt it to the shape of the land characteristics.

The terrain slope influences the electrical output and the construction cost of large-scale PV plants [28]. Excessive hard works on the land that produce changes in its natural landscape must be avoided, therefore relatively flat areas are required. A common criterion for the maximum terrain slope accepted in this type of installations has not yet been reached. For example, Yushchenko et al. [29] have proposed the criterion of 5.71 (°) (or 10%) of terrain slope, Alami et al. [30] have accepted a maximum of 5% terrain slope and IRENA [31] has proposed the criterion of 11.3 (°) (or 20%).

Another factor which influences the selection of the installation site of a PV plant is its elevation. High altitude locations have less flora and fauna species [32] and they receive more solar irradiance, but there the electricity transmission network is sparse [32]. According to the data from the literature, 1500 (m) elevation can be considered to be the maximum one [33].

2.2. Mounting system

Mounting systems allow PV modules to be securely attached to the ground. The installation of racking systems with a fixed tilt angle is less difficult, cheaper and requires less maintenance. However, the racking systems with a variable tilt angle generate more energy. Systems with a dual-axis tracker are used to get a higher accuracy but they are more expensive. The production definitely is not the only thing that matters here. As the PV modules are now more affordable than ever, it would be cheaper to install more PV modules than to include a dual-axis tracker or a single-axis tracker.

In this paper, the mounting system used is the ground-mounted photovoltaic one with an annual fixed tilt angle. In this type of mounting system, various rack configurations can be used: $1V \times N_{PV}$, $2V \times N_{PV}$, $3V \times N_{PV}$, $2H \times N_{PV}$, $3H \times N_{PV}$, ...Where, the numbers 1, 2, 3, ...represent the number of the vertical consecutive modules in each row of the system and the letter, V refers to the rack configuration in which the magnitude L_{PV} is the reference for the tilt angle, the letter H stands the configuration in which W_{PV} is used as such reference, (W_{PV} is the module width, L_{PV} is the module length and N_{PV} is the number of PV modules per row).

The structural system is composed of columns (1), beams (2), purlins (3) and braces (4). The column is the seat for the beam. The beam and the purlin are pinned joint. A beam can be connected to one column or two columns. Fig. 1 shows the parts of the most commonly used rack configurations, $2V$ and $3V$ configurations.

The mounting systems can be classified according to the number of mounting columns. Two types of mounting systems are commonly used [34]: one-column mounted systems and two-column mounted systems. In this case, the two-column mounted system has been used in the study.

The racking systems with a fixed tilt angle are always South-oriented (in the Northern hemisphere) [35].

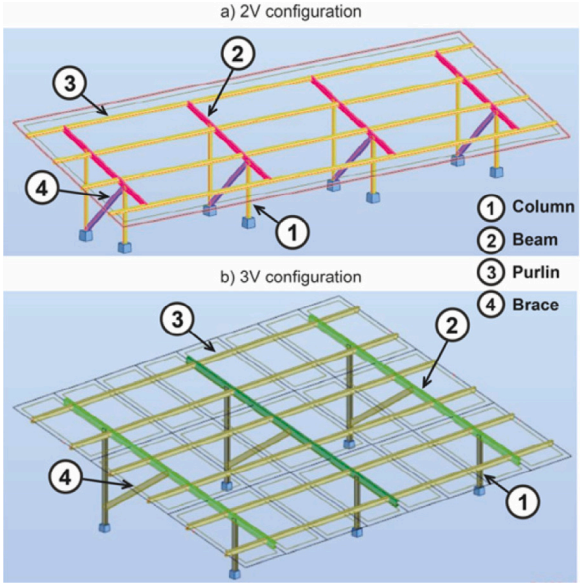

Fig. 1. Solar array mounting frame structural arrangement types.

2.3. Solar irradiance estimation model

The solar irradiance received on the horizontal surface makes an impact about the decision of investors about the suitable sites for large-scale PV plants. Obviously, the more solar irradiance is received, the higher the electricity generation will be. In order to select the suitable sites for large-scale PV plants, the use of a solar irradiance estimation model is needed. In addition, the calculation of the optimum tilt angle of PV modules also depends on the accuracy of solar irradiance estimation.

Ground-level meteorological stations provide accurate data but the number of these stations is small. Therefore the use of models has become widespread although the results they give are approximate. Many methods for estimating solar irradiance are available in the literature. Some authors use clear-sky models [36]. The others use the analysis of satellite images [37] or temperature based methods [38] instead.

In order to determine the annual distribution of solar irradiance in a specific site, in this work the method presented by [39] has been used. This method determines the two components of the global solar irradiance on a horizontal surface. For this purpose, it uses (i) the Hottel's model [40] for estimating the beam solar irradiance transmitted through a clear atmosphere, (ii) the Liu and Jordan's model [41] for determining the diffuse solar irradiance that comes from a clear-sky, (iii) satellite databases [42] for obtaining long-term data in a large area and (iv) Fourier series approximation for correcting the clear-sky models and adapting them to the variations of the local cloud cover distribution. Therefore, with the theoretical beam (or diffuse) solar irradiance on a horizontal surface, this method calculates the solar irradiance adjusted to the climatological conditions of a specific location.

This method has been validated in different places worldwide [39]. For this purpose, it has been compared with current data obtained from ground-level stations [43]. Therefore, it can be assumed that the use of this method makes it possible to obtain valid results for the study of PV plants [15]. Adjusted total solar irradiance on a horizontal surface $\mathbb{I}_h$ (W/m^2), can be decomposed into two components: the adjusted beam solar irradiance $\mathbb{I}_{bh}$, and the adjusted diffuse solar irradiance $\mathbb{I}_{dh}$, [44]:

$$\mathbb{I}_h(n,T) = \mathbb{I}_{bh}(n,T) + \mathbb{I}_{dh}(n,T) \quad (1)$$

The value of each component depends on the day of the year n, and the solar time T(h). These adjusted irradiances will be later on used to calculate the energy.

3. Methodology

The design of a PV plant as a whole is complicated as there are many variables to be considered [33] such as the geographical location, the local weather conditions, the available land area, the land shape, the land slope, the land orientation, the availability of water for cleaning the PV modules in order to maintain their efficiency, the availability of a power grid and the accessibility to it, the rack configuration, the commercial PV modules, the commercial inverters, etc. Researchers have concluded that the site selected to install a PV plant must have a good accessibility, be flat and have high levels of solar irradiance [30]. After the analysis of the input parameters, the designer has to select components of the installation such as the distribution of PV modules, the number of PV modules, the type of PV modules, the type of rack configuration, the number of rack configurations, the number of inverters, the type of inverters, etc. Therefore, this paper has been limited to consider those aspects related to maximize the number of PV modules for a particular available land area. For this purpose, the available area, the shape, the slope and the orientation of the land will be taken into account.

The combination of GIS tools and $Mathematica$™software is a new approach that can be very useful to solve the complex problem of the optimization of the distribution of PV modules in large-scale PV plants. Under this framework, the proposed methodology will be developed. This methodology consists of the following steps: (i) Identifying the geographical location of the project; (ii) Getting the UTM (Universal Transverse Mercator) coordinates of the available land area; (iii) Converting the UTM coordinates into the $Mathematica$™software; (iv) Choosing the rack configuration; (v) Choosing the objective function; (vi) Shadows study; (vii) Development of the optimization algorithm; (viii) Structural analysis of the mounting system; and (ix) Cost analysis. A flowchart outlining the proposed methodology is shown in Fig. 2.

The assumptions made in this study are the following:

(i) The goal of the study is to maximize the PV plant energy production. For this purpose, the optimal distribution of PV modules will be determined for each particular available land.

(ii) The geographical location is not the aim of this study.

(iii) The land has any irregular shape and it is flat. The land selection is not the aim of this study.

(iv) Racking systems with an annual fixed tilt angle will be used in this study.

(v) The choice of commercial PV module is limited to one type.

(vi) The choice of rack configuration is limited to these two types: $2V \times 12$ and $3V \times 8$.

(vii) A transversal and a longitudinal installation distance between PV modules of 0.025 (m), due to clamps, are considered.

(viii) A transversal installation distance (e_t) is considered in order to facilitate the passage between the mounting systems of PV modules.

(iv) A minimal longitudinal maintenance distance (e_l^m) between the rows of PV modules in order to allow a proper inspection, cleaning, and maintenance is considered.

(x) The environmental impacts and socioeconomic benefits are not the goals of this study.

(xi) The work does not give any attention to incentives and financing.

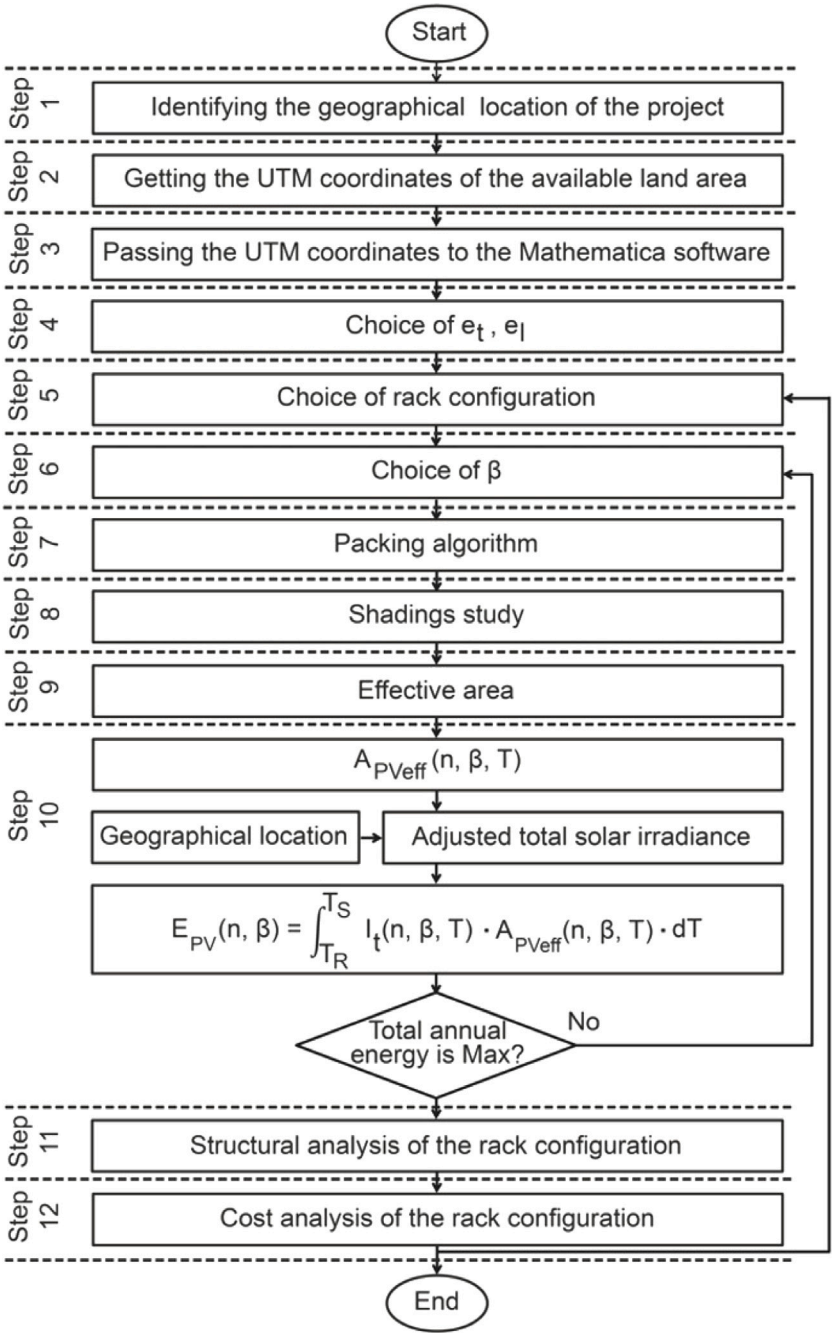

Fig. 2. A flowchart outlining the proposed methodology.

3.1. Obtaining the UTM coordinates of the available land area

Previous studies are only based on rectangular shape lands for the installation of large-scale PV plants [45], although the majority of large-scale PV plants are installed in irregular shape areas. Therefore an irregular shape land is considered in this methodology.

The surface occupied by the large-scale PV plant is calculated on the basis of the UTM (Universal Transverse Mercator) coordinates. The Geographic Information System (GIS) has been used in the determination of UTM coordinates in the area selected for the installation of the PV plant. In particular, an open-source geographic information system software has been used, this is the $QGIS$. This software allows the conversion, visualization and analysis of geospatial data. The wide range of external plugins and their free availability are advantages that make the use of $QGIS$ favoured by many researchers [46,47].

The main tasks of $QGIS$ can be summarized as: downloading of Landsat images, preprocessing of Landsat images and determining UTM coordinates. The National Geographic Information Center of the Government of Spain [48] provides database on Landsat images. This study uses $QGIS$ software to extract the UTM coordinates and the slope of the land.

3.2. Passing the UTM coordinates to the Mathematica™ software

As it has been mentioned before, in order to get the dimensions of the land area, firstly a Geographical Information System is used, in this work this is the $QGIS$™, because it is a free software with an open code. Then, on the land area, a certain number of points that will define the shape of this land area as a polygon $p[i], i = 1, 2, \ldots, n.$ are selected. In each particular case the user will select the most adequate number of

points to form a polygon which adapts itself with sufficient precision to the limits of the land area. The user can also draw inside this polygon any convenient path. Each one of these points is defined by two values: $utmEasting$ and $utmNorthing$ [49]. The user also knows the UTM Zone and the elevation of the land area.

The next step is to use the $Mathematica$™software. With the following orders the polygonal projection P is easily obtained [49]:

$$P = \text{Polygon}[\text{Table}[p[i], \{i, 1, n\}]] \tag{2}$$

Then the projection P should be inscribed in a rectangle R. For convenience, the lower left point of R ($O = R[[1]]$) is taken as the origin O and both R and P are moved. An easy and convenient way to do this could be [49]:

$$R = \text{BoundingRegion}[\{\text{Table}[p[i], \{i, 1, n\}]\},\text{“MinRectangle”}] \tag{3}$$

$$\overline{R} = \text{TransformedRegion}[R,\text{TranslationTransform}[-O]] \tag{4}$$

$$\overline{P} = \text{TransformedRegion}[P,\text{TranslationTransform}[-O]] \tag{5}$$

As a result of this, the area $\overline{P}$ has been defined.

Note: It is important to know that the use of the order TransformedRegion is a previous fundamental step to be able to later on use the order RegionMember and verify in an easy way the correct packing.

3.3. Choice of rack configuration of the mounting structure

The mounting structure allows the PV modules to be securely attached to the ground with a fixed tilt angle. The mounting systems can be made of aluminium alloy, galvanized steel or stainless steel. Although, in large-scale PV plants the galvanized steel is generally used [16].

Two rack configurations are used in practical installations: $2V \times 12$ and $3V \times 8$ [16]. These are the configurations that have been studied in this paper. These configurations modelled by means of the AutoDesk Robot Structural Analysis are shown in Fig. 1.

3.4. Packing algorithm: Maximization of total modules area

Many optimization alternatives can be performed in a PV plant. In this first phase of the study, the objective function considered for designing the PV plant is set for maximizing the total PV modules area (A_{TPV}). The total PV modules area (A_{TPV}) is represented in Eq. (6):

$$A_{TPV} = \sum_{i=1}^{N_{PV}} W_{PV} \cdot L_{PV} \tag{6}$$

where N_{PV} is the number of PV modules, W_{PV} is the width of a PV module (m), and L_{PV} is the length of a PV module (m).

For this purpose, some restrictions have to be taken into account:

1. A transversal and a longitudinal installation distance between PV modules of 0.025 (m) have been considered, due to the clamps.
2. A transversal installation distance (e_t) has been considered to get the appropriate PV modules installation.
3. A longitudinal maintenance distance (e_l^m) between the rows of PV modules has also been considered in order to allow a proper inspection, cleaning, and maintenance.

The presented packing algorithm includes the optimization of the number of rows in the mounting systems, the row width, the row height and the space between adjacent rows. In this paper each possible tilt angle β of the PV module has been analysed. As regards the possible azimuth angles of the PV module, the majority of the authors consider $\gamma = 0$ (°) [35]. Furthermore, in order to assert this election, a previous study of these authors has reached the conclusion that the influence of the tilt angle is much bigger than that of the azimuth angle [27].

Fig. 3 shows a row of South-orientated PV modules ($\gamma = 0°$). It can be easily deduced that for the longitudinal component it comes true:

$$\tan\theta_l = \frac{\cos\alpha_s \cos\gamma_s}{\sin\alpha_s} = \frac{\cos\gamma_s}{\tan\alpha_s} = \tan\theta_z \cos\gamma_s \tag{7}$$

where α_S is the height angle of the Sun (rad), θ_z is the zenith angle of the Sun (rad) and γ_S is the azimuth of the Sun (rad).

In order to minimize shading effects this study applies the Spanish Government Technical Report [50]. This standard states that the distance between PV modules has to guarantee a minimum of 4 h of sunshine around noon on the Winter solstice. Here θ_{l0} stands for the solar longitudinal incidence angle given by (7) on December 21 at 10 : 00. From Fig. 3 it is immediately obtained that the longitudinal spacing in order to fulfil the previous standard (e_l^{st}) and to avoid the shading between two consecutive rows of the mounting systems is:

$$e_l^{st} = S\frac{\tan\beta}{\cot\theta_{l0}} = L\frac{\sin\beta}{\cot\theta_{l0}} \tag{8}$$

where $S = L\cos\beta$ is the projection of L on the horizontal plane. The final value that should be imposed as the longitudinal distance (e_l) is:

$$e_l = \max[e_l^m, e_l^{st}] \tag{9}$$

so that it guarantees not only a distance that allows the maintenance of the PV system but also the standard fulfilment.

The packing scheme consists of placing rows of mounting systems to the East–West direction, South-wards orientated and with dimensions $W \times L$ inside the available land area $\overline{P}$.

Throughout this phase of the process, the vertical projection of each one of the mounting systems with dimensions $W \times S$ should be considered. All these rectangles R_{ij} are fixedly orientated to the Sun. Due to the method that has been used to get the dimensions of the land area, the North–South orientation is already given by the $QGIS$, and as a result of that the rectangle $\overline{R}$ sides have been taken as the reference axes ($x - y$) the N-S direction as the positive axis y. Moreover, with no loss of generality, the lower left corner of the rectangle $\overline{R}$ where $\overline{P}$ is inscribed, is taken as the origin O. A base rectangle R_{11} is defined using the vertex A on the origin O of the rectangle $\overline{R}$ (see Fig. 4):

$$R_{11} : \{A(0,0), B(W,0), C(W,S), D(0,S)\} \tag{10}$$

It is defined:

$$\Delta x = W + e_t; \quad \Delta y = S + e_l \tag{11}$$

The packing pattern adds in W-E direction and in N-S direction as many rectangles R_{ij} as possible:

$$\begin{aligned} R_{ij} : \{&A((j-1)\Delta x, (i-1)\Delta y), \\ &B((j-1)\Delta x + W, (i-1)\Delta y), \\ &C((j-1)\Delta x + W, (i-1)\Delta y + S), \\ &D((j-1)\Delta x, (i-1)\Delta y + S)\} \end{aligned} \tag{12}$$

With this purpose, the order RegionMember [49] has been used and a check on how many mounting systems can be packed in $\overline{P}$ has been made.

Eventually, the restriction on the fact that the vertex A of the basis rectangle R_{11} is O has been eliminated. To get this, the algorithm chooses different points for the vertex A of R_{11} inside the area $\Delta x \times \Delta y$ highlighted in Fig. 4 with the help of a discrete shadow m. Outside this area $\Delta x \times \Delta y$ this arrangement repeats again.

Once the m^2 possible combinations have been analysed, the algorithm (been fixed W and L, fixed e_l^m and because of the fact that θ_{l0} is deduced from the standard) provides for each tilt angle β the best arrangement of the mounting systems, this is, the maximum of $A_{PV}(\beta)$. The algorithm also shows the maximum number of panels $np(\beta)$ and how many of them are never affected by shadows, $npss(\beta)$, as they are the first to receive the sunlight from the South.

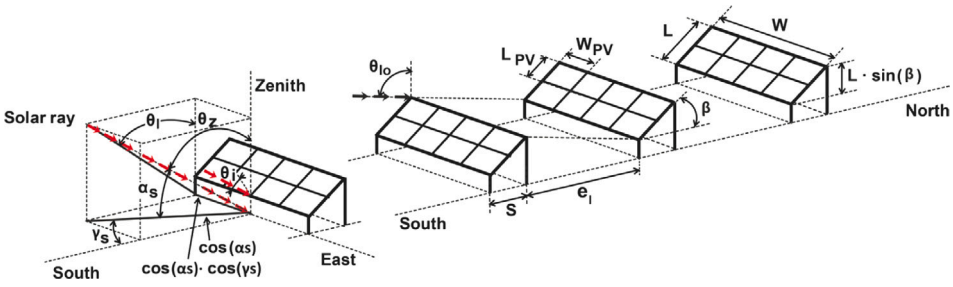

Fig. 3. Longitudinal and transversal study of the installation.

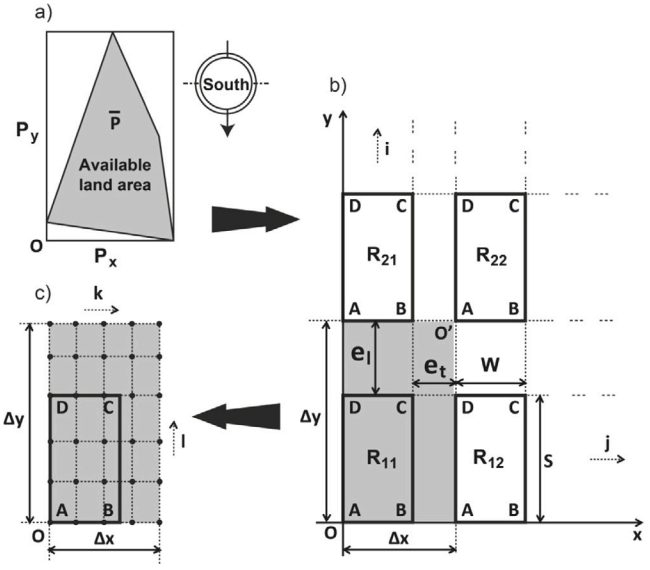

Fig. 4. Packing algorithm.

3.5. Shading study: Maximization of effective modules area

Next, in this section, the shadows produced in between the rows of mounting systems are going to be considered. This point is certainly a fundamental aspect that has been deeply studied.

In Section 4 (Results and discussions) it is shown that the fulfilment of the standard [50] given by (8) guarantees the total absence of shading effects in between the rows of mounting systems for a certain range of hours (which are function of θ_{l0}) for each day throughout the year. $[T_1(n), T_2(n)]$ are named operating hours of the PV system. These are hours through which the absence of shading is guaranteed and simultaneously the $\cos\theta_i \geq 0$.

On the contrary, when the transversal angle θ_l is bigger than θ_{l0} (this is, inside $[T_R(n), T_S(n)]$ but outside $[T_1(n), T_2(n)]$) a shading effect is produced and, as it comes from Fig. 5, the value of the shadow B, produced by one row of mounting systems on the next one is given by:

$$B(n,\beta,T) = \frac{\sin(\theta_l - \theta_{l0})}{\cos(\beta - \theta_l)} L \sin\beta \sec\theta_{l0} \tag{13}$$

This deduction is simply based on the Law of sines and on an accurate calculation. The shading effect has obviously been considered when calculating the energy daily obtained from $T_R(n)$, sunrise solar time (h), up to $T_S(n)$, the sunset solar time (h).

Once all the previous calculations have been made, it results that the effective PV modules area (A_{PVeff}) is:

$$A_{PVeff}(n,\beta,T) = A_{TPV}(\beta) - W.B(n,\beta,T)\cdot(np(\beta) - npss(\beta)) \tag{14}$$

It evidently now shows that A_{PVeff} depends not only on β, as it happens to A_{TPV} but also on the day n and on the time T. This fact indicates the way of calculating the energy that is shown next.

3.6. Maximization of energy incident on a tilted surface

In a previous paper [27], where the shading effect had not been taken into account, the energy calculation was made in a simpler way. The calculation of the adjusted irradiation curve as a function of the tilt, $\mathbb{H}_t(\beta)$ and multiplying by the total area $A_{TPV}(\beta)$ obtained from the packing algorithm was enough. In this simple case, the maximum β^*, in the curve which represents the total energy, was calculated:

$$E_{PV}(\beta) = \mathbb{H}_t(\beta)\cdot A_{TPV}(\beta) \tag{15}$$

But the procedure in the current work is different.

Following previous studies ([51–53]) the isotropic model of Liu and Jordan [54] for the diffuse and the ground reflected solar irradiation (Wh/m^2) on a tilted surface has been used in this work. Therefore the energy $E_{PV}(n,\beta)$ (Wh) has been calculated with the integral [44]:

$$E_{PV}(n,\beta) = \int_{T_{R(n)}}^{T_{S(n)}} \left[\mathbb{I}_{bh}(n,T)\cdot\frac{\cos\theta_i}{\cos\theta_z} + \mathbb{I}_{dh}(n,T)\cdot\left(\frac{1+\cos\beta}{2}\right) + \right.$$
$$\left. + \left(\mathbb{I}_{bh}(n,T) + \mathbb{I}_{dh}(n,T)\right)\cdot\rho_g\cdot\left(\frac{1-\cos\beta}{2}\right)\right]\cdot A_{PVeff}(n,\beta,T)\,dT \tag{16}$$

where the adjusted horizontal irradiances (W/m^2) ($\mathbb{I}_{bh}, \mathbb{I}_{dh}$) have been calculated using the method proposed by [39]. In Eq. (16), n is the day of the year (day), β is the tilt angle (rad), θ_z is the zenith angle of the Sun (rad), ρ_g is the ground reflectance (dimensionless), T is the solar time (h), T_R is the sunrise solar time (h), T_S is the sunset solar time (h) and θ_i is the incident angle (rad) calculated as [44]:

$$\begin{aligned}\cos\theta_i &= \sin\delta\cdot\sin\lambda\cdot\cos\beta - \sin\delta\cdot\cos\lambda\cdot\sin\beta\cdot\cos\gamma \\ &\quad + \cos\delta\cdot\cos\lambda\cdot\cos\beta\cdot\cos\omega \\ &\quad + \cos\delta\cdot\sin\lambda\cdot\sin\beta\cdot\cos\gamma\cdot\cos\omega + \cos\delta\cdot\sin\beta\cdot\sin\gamma\cdot\sin\omega\end{aligned} \tag{17}$$

where δ is the solar declination (rad), λ is the latitude (rad), β is the tilt angle (rad), γ is the azimuth angle (rad), and ω is the hour angle (rad). In this last Eq. (17), it is necessary to take into account two conditions proposed by [44]: (i) the incident angle may exceed 90°, which means that the Sun is behind the surface and (ii) the Earth is not blocking the Sun. With regard to γ, the azimuth angle (rad), the value 0 (rad) [27] has been taken as previously mentioned.

Eventually, the total *annual* energy for each tilt angle β has been calculated:

$$E_a(\beta) = \sum_{n=1}^{365} E_{PV}(n,\beta) \tag{18}$$

and from this curve, $E_a(\beta)$ $(Wh/year)$, the optimum β^* for each rack configuration immediately results.

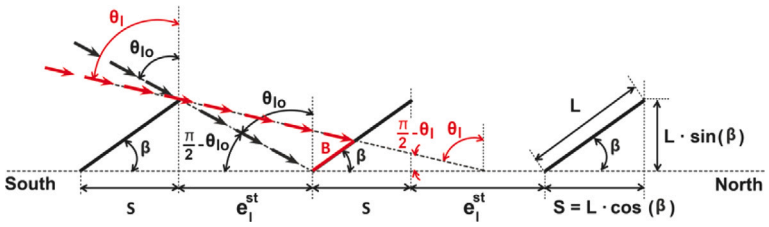

Fig. 5. Shading calculation.

3.7. Structural analysis of the mounting system

The steel structure designed for the mounting system must be able to support its weight, the weight of the PV modules, the weight of accumulated snow and the wind loading, or combinations thereof during its lifetime.

For the structural analysis the standards and the codes listed below have been used: (i) UNE-EN 1990: 2019, Basis of structural design [55]; (ii) UNE-EN 1991-1-7: 2018, Actions on structures [56]; (iii) UNE-EN 1993-1-9:2013, Design of steel structures [57]; (iv) UNE-EN ISO 1461:2010, Hot-dip galvanized coatings on fabricated iron and steel articles [58]; (v) UNE-EN ISO 14713-1:2017, Zinc coatings - Guidelines and recommendations for the protection against corrosion of iron and steel in structures [59]; (vi) CTE DB-SE-A: 2006, Structural safety - Steel structures [60]; (vii) CTE DB-SE-AE: 2006, Structural safety - Actions on buildings [60].

The accurate estimation of the magnitudes of these loads is an important aspect of this analysis. The structural weight can be directly calculated with the software itself.

To calculate the load due to the weight of the PV modules the Eq. (19) can be used:

$$q_{PV} = \frac{W_{ePV}}{A_{PV}} \tag{19}$$

where W_{ePV} is the weight of the PV module (kg) and A_{PV} is the area of a PV module (m^2).

To calculate the load due to the snow, the following considerations have been made:

(i) How is distributed the load of the accumulated snow.

(ii) The load concentrations are considered to be negligible.

In the annex E of the code CTE DB-SE-AE: 2006, Structural safety - Actions on buildings [60] the snow load for each state zone and for each altitude is detailed.

The method for calculating the wind load is defined in code CTE DB-SE-AE [60]. For this purpose the Eq. (20) can be used [60]:

$$q_e = q_b \cdot C_e \cdot C_p \cdot C_{prob} \tag{20}$$

where q_e is the static pressure (kN/m^2), q_b is the basic velocity pressure for the reference speed established in the code (kN/m^2), C_e is the exposure factor, C_p is the pressure coefficient, and C_{prob} is the probability factor.

According to the annex D of CTE DB-SE-AE [60], q_b is determined from the expression:

$$q_b = \frac{1}{2} \cdot \rho \cdot v_b^2 \tag{21}$$

where ρ is the air density (Kg/m^3), which value is determined as 1.25 (Kg/m^3) and v_b is the basic wind velocity (See Table D.1 CTE DB SE-AE [60]).

C_p is defined in Paragraph D.3 CTE DB SE-AE [60] .

C_{prob} is defined in Annex D.1 of CTE DB-SE-AE [60] depending on the period of service of the considered element.

C_e can be defined as:

$$C_e = k^2 \cdot \left[\ln^2 \left(\frac{z}{L_e} \right) + 7 \cdot \ln \left(\frac{z}{L_e} \right) \right] \tag{22}$$

where z is the height on the ground (m) and k and L_e are parameters that depend on the land (See Table D.2 CTE DB-SE-AE [60]).

The components of the structure are designed for critical scenarios. These scenarios are identified using structural analysis for different load combinations. Load combinations specified by CTE DB-SE-A [60] are tabulated in Table 2.

where W_{eS} is the weight of the structure, W_{ePV} is the weight of the PV module, S_L is the snow load and W_L is the wind load.

Combinations of the Ultimate limit state for calculating the sections dimensions in relation with the maximum profiles resistance and the joins have been used. On the other hand, in order to calculate the sections dimensions in relation with the existing strains and the foundation dimensions, combinations of Serviceability limit state have also been used.

The selection of the foundation for ground mounted PV systems is another important aspect to be considered. The selection of the foundation is an essential factor for a cost-effective installation of the PV module support structures. A proper study of the underground conditions is necessary for the selection of the appropriate type of foundation. There are four types of foundations commonly utilized in large-scale PV plants. These types of foundations ordered from the lower to the higher cost-effective installation are [16]: driven piles, earth-screws, helical piles and ballasted foundations. In this work, driven piles have been used.

3.8. Cost analysis

The total cost of a large-scale PV plant during its lifetime is the sum of two costs: the initial investment cost and the operation and maintenance costs.

The initial investment cost can be calculated by Eq. (23) [61]:

$$C_i = N_{PV} \cdot C_{PV} + N_{inv} \cdot C_{inv} + C_L + N_{MS} \cdot C_{MS} + C_{cb} + C_T + C_{pd} + C_M \tag{23}$$

where N_{PV} is the total number of PV modules, C_{PV} is the unit cost of a PV module (€/unit), N_{inv} is the total number of inverters, C_{inv} is the unit cost of the inverter (€/unit), C_L is the cost of the land area (€), N_{MS} is the total number of mounting structures, C_{MS} is the unit cost of the mounting structure (€/*unit*), C_{cb} is the cost of the cable (€), C_T is the cost of the transformer (€), C_{pd} is the cost of the protection devices (€), and C_M is the cost of the monitoring system (€). Obviously, these costs depend on specific parameters of the site.

Despite the lack of standardization [5] for the Operation and Maintenance costs, the National Renewable Energy Laboratory recommends assuming an annual cost of 0.5% of the total initial cost for large systems and one of 1% for small ones [62]. Moreover, Mortensen [6] suggests that operation and maintenance costs with tracking systems are double those of fixed-tilt ones.

The available land area is a constant parameter in this work, therefore it can be considered that the equation terms (23): C_L, C_{cb}, C_T, C_{pd}, C_M, and N_{inv} stay the same for all the studied rack configurations. Although, the C_{inv} could slightly vary with each configuration, its value has also been considered to be constant. Therefore, the parameters of Eq. (23) subject to variation are: N_{PV}, C_{PV}, N_{MS} and C_{MS}. The N_{PV} and N_{MS} parameters are obtained by the application of the proposed algorithm. C_{PV} is given by the PV modules-maker. To get C_{MS} it is

Table 2
Classification of load combinations.

Designation	Ultimate limit state	Designation	Serviceability limit state
ULS 1	$1.35\cdot(W_{eS}+W_{ePV})$	SLS 1	$(W_{eS}+W_{ePV})$
ULS 2	$1.35\cdot(W_{eS}+W_{ePV})+1.5\cdot W_L+0.75\cdot S_L$	SLS 2	$(W_{eS}+W_{ePV})+W_L+0.5\cdot S_L$
ULS 3	$0.8\cdot(W_{eS}+W_{ePV})+1.5\cdot W_L$	SLS 3	$(W_{eS}+W_{ePV})+W_L$
ULS 4	$1.35\cdot(W_{eS}+W_{ePV})+0.9\cdot W_L+1.5\cdot S_L$	SLS 4	$(W_{eS}+W_{ePV})+0.6\cdot W_L+S_L$

necessary to know the weights of the different elements of the structure which are get from the structural analysis.

The assessment of the economic viability of a project is a key element to make an investment decision. The objective of the economic viability is to measure the economic value of each one of the proposed rack configurations. To evaluate the economic performance of the proposed rack configuration, the levelized cost of the produced electrical energy ($LCOE$) is calculated. The $LCOE$ in ($€/kWh$) can be defined as the ratio between the life-cycle cost of the PV system and the whole life produced energy. Ref. [63] has provided an equation to calculate the $LCOE$ for a PV system. This equation is given in Eq. (24) below:

$$LCOE=\frac{\sum_{i=0}^{I}\left[C_i/(1+r)^i\right]}{\sum_{i=0}^{I}\left[E_i/(1+r)^i\right]} \tag{24}$$

where C_i is the net cost of the project for i (€), E_i is the total electrical energy output for i (kWh), I is the lifetime of the project ($years$), r is the discount rate for i, and i is the year.

The net cost of the project involves: the initial investment cost, the operation and maintenance costs and the interest expenditure if it is debt financed. The initial investment cost can be calculated with the Eq. (23). The 0.5% of the initial investment has been assumed for the operation and maintenance costs.

The total electrical energy output at the ith year could be calculated as following:

$$E_i=S_i\cdot\eta\cdot(1-d)^i \tag{25}$$

where E_i is the total electrical energy output at the ith year (kWh), S_i is the availability of solar resource at the ith year (kWh), η is the performance factor, d is the annual degradation rate, and i is the year. The terms η, d, and i can be considered to have the same value for all the studied rack configurations, because the same type of PV modules has been used.

The $LCOE$ implicitly depends on site specific variables such as the power capacity, the PV technology and the location. The PV technology used and the location are the same. Therefore, only the power capacity varies. In this work, the "$LCOE$ efficiency" is introduced as the ratio between the $LCOE_{2V}$ with $2V$ configuration and the $LCOE_{3V}$: with $3V$ configuration:

$$\eta_{LCOE}=\frac{LCOE_{2V}}{LCOE_{3V}} \tag{26}$$

Notice that an η_{LCOE} value greater than 1 implies that the $2V$ configuration is less efficient than the $3V$ configuration.

4. Results and discussions

In this work, the optimal distribution of PV modules in a PV plant using a packing algorithm is developed to determine the maximum amount of energy captured by all the PV modules. The optimum distribution of PV modules is analysed for a geographic location. Specifically, a PV plant (Sigena I) with a fixed tilt angle located in Villanueva de Sigena (Spain), with latitude $41°44'19''N$, longitude $0°1'37''W$ and altitude 235 (m) is studied in this work. The available land area has an irregular shape. Fig. 6 shows an aerial photograph of the installation, as well as the parcel $\overline{P}$ and the rectangle $\overline{R}$ obtained with the method described in Section 3.2. The Table 2 summarizes the actual parameters of the Sigena I PV plant. Based on the described methodology, this section shows the main results of the simulations for the different mounting system configurations.

The analysis has focused on three particular mounting system configurations. The first one is the current Sigena I PV plant configuration which is $2V\times 12$ configuration with a tilt angle of 30 (°) ($2V^A$). The second one is a $2V\times12$ configuration obtained by applying the proposed methodology ($2V^P$). And the third one is a $3V\times 8$ configuration obtained by applying the proposed methodology ($3V^P$). In each one of these configurations 24 PV modules have been used. The type of PV module that has been chosen is the model JAM72S20 440-465/MR manufactured by JASolar, which has a rated maximum power of 450 (W) and dimensions of 2120×1052 (mm).

The optimization algorithm has been implemented with $Mathematica^{TM}$ software. A specific $Mathematica^{TM}$ code calculates the direct, the diffuse, and the reflected components of the solar irradiance. This code uses the satellite-derived $PVGIS$ data [42] as inputs of monthly-averaged beam and diffuse solar irradiation. The effect of the weather conditions is taken into account with the method proposed by [39].

The angle θ_{l0} imposed by the standard [50] on the solar longitudinal incidence angle for the location of Sigena is 68.31 (°). Fig. 7 shows three curves. Firstly, the black curve represents the dawn and the sunset hours of each day through the year: $T_R(n)$ and $T_S(n)$. Secondly, by using Eq. (17), the hours through which the $\cos\theta_i\geq 0$ have been calculated for each day, in order to ensure that the Sun faces towards the PV surface. These values are represented with the red curve. Finally, the hours of each day through the year in which it is fulfilled that $\theta_{l0}=68.31$ (°): $T_1(n)$ and $T_2(n)$ have been calculated by means of (7), and they have been represented with the blue curve. In between $[T_1(n), T_2(n)]$ the absence of shading between the PV modules is guaranteed. This graph shows that the black curve and the blue one are the same curve when the declination δ is positive. This occurs in the case of the selected location between the 80th and the 267th days.

4.1. Optimum distribution of PV modules.

Next, in this example, a longitudinal spacing for maintenance $e_l^m=4$ (m) and a transversal installation distance of $e_t=0.30$ (m) have been fixed as well as a gap of 25 (mm) due to the clamps. In the $2V$ configuration it is fulfilled that $W=12\cdot1052+11\cdot25$ (mm) and $L=2\cdot2120+25$ (mm), whereas in the $3V$ configuration it is fulfilled that $W=8\cdot1052+7\cdot25$ (mm) and $L=3\cdot2120+2\cdot25$ (mm). Once these values have been fixed, as well as θ_{l0} obtained with the standard, the Packing algorithm provides for each tilt angle β the best arrangement of PV modules and the maximum value of the total modules area $A_{TPV}(\beta)$. A variation interval of the tilt de of $\beta\in[0,45]$ (°) has been considered.

Fig. 8 shows the total PV modules area as a tilt function, $A_{TPV}(\beta)$ for both $2V$ and $3V$ configurations. The type of the rack configuration has a great influence on the total PV modules area. For the same value of β the $3V$ configuration is always more advantageous than the $2V$ one. There are several reasons that cause such advantage. L and W are two of the parameters that give to $3V$ configuration its advantage.

Firstly, the length L in a $3V$ configuration (a 50% bigger than that in a $2V$ configuration) is the main factor that gives this advantage. It reduces the number of passages required for maintenance in the $3V$ configuration. Taking into account that the value of the longitudinal spacing for maintenance, $e_l^m=4$ (m) is very high, it has a great influence on the result because it represents a useless area.

Fig. 6. Aerial photograph of the PV installation and parcel $\overline{P}$.

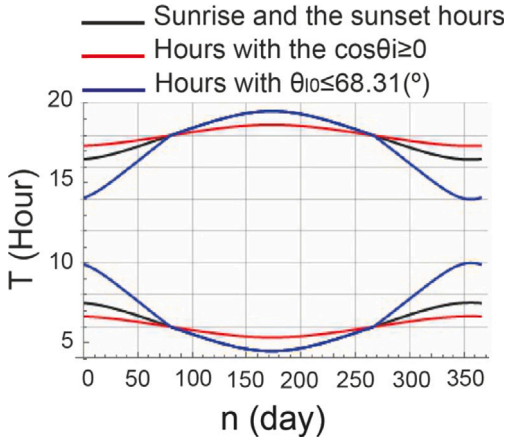

Fig. 7. Operating hours of the PV system with shading and no shading.

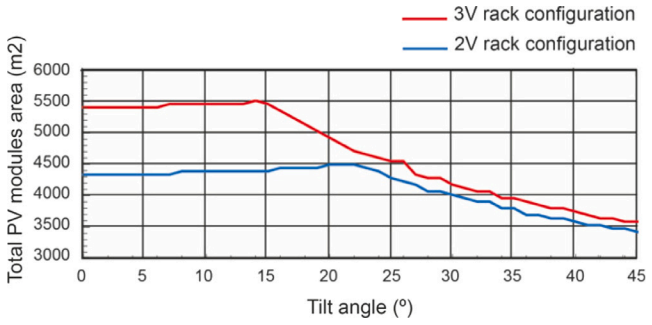

Fig. 8. Total PV modules area, $A_{TPV}(\beta)$.

Secondly, although the width W of the mounting system in a $2V$ configuration is 1.5 times bigger than that in a $3V$ configuration, the transversal space for the passage is $e_t = 0.30$ (m) and therefore its influence is much lower. So, although the $3V$ configuration requires more passages, this fact is largely counterbalanced by the ease of packing in the East–West direction that has the $3V$ configuration.

On account of that, L is a factor with more influence than W on the packing.

Fig. 8 aids the analysis of β which is the next parameter. For very low values of β, a small increase of the area $A_{TPV}(\beta)$ is produced as the value of β increases. This occurs because more modules can be packed without producing shadows between the adjacent rows. Although, once the maximum value has been obtained, Fig. 8 shows how the increase of β rapidly decreases the number of PV modules installed and, consequently, the area $A_{TPV}(\beta)$. This is so because an increase of β implies an enlargement of the distance between the rows of PV modules in order to fulfil the standard (e_l^{st}) of the Spanish Government Technical Report [50] and to avoid the shading between two consecutive rows of the mounting systems.

The values of β that produce the maximum total area $A_{TPV}(\beta)$ of PV modules, are the same as the values of β that give values of the parameter longitudinal spacing e_l that are close to the minimum value of maintenance $e_l^m = 4$ (m). This allows the users to predetermine in a simple way a range of appropriate values of β. This is a fact important enough to be highlighted as result of this study. The area $A_{TPV}(\beta)$ is another important factor, but not the only one, in order to maximize the total energy.

In the next step of the algorithm the effective PV modules area $A_{PVeff}(n, \beta, T)$ has been calculated using Eq. (14). Fig. 9 shows the results obtained in both $2V$ and $3V$ configurations for the particular case of $\beta = 22$ (°). It shows that in the Interval $[T_1(n), T_2(n)]$ there is no shading and at the same time $A_{TPV} = A_{PVeff}$ whereas in the interval $[T_R(n), T_1(n)] \cup [T_2(n), T_S(n)]$ the shading effect causes A_{PVeff} to appreciably decrease. This happens in the case of the selected location all the days but those between the 80th and the 267th days, when the declination δ is positive. Fig. 9 shows that the type of the rack configuration has a great influence on the total PV modules area, in this case for $\beta = 22$ (°). This value has been chosen because it is the optimum β for the $2V$ configuration and despite that, the $3V$ configuration gets the best results.

Following, $E_{PV}(n, \beta)$ has been calculated using Eq. (16) and the obtained surfaces are shown in Fig. 10. This figure shows how the increase of β decreases the annual energy. This is so because the increase of β implies an enlargement of the distance between the rows of PV modules and therefore, a reduction in the number of the PV modules installed. The range of values of β with which high values of annual energy are obtained is the same as the parameter longitudinal spacing for maintenance that has a minimum value of 4 (m).

Eventually, the annual sum of energy for each tilt β has been calculated and the curves $E_a(\beta)$ are shown in Fig. 11.a for $e_l^m = 4.00$ (m). From these curves the optimum β^* for each rack configuration is immediately obtained: for the $2V^P$ it comes out $\beta^* = 22$ (°) with a $E_a = 8436.96$ (MWh) and for the $3V^P$ it comes out $\beta^* = 14$ (°) with a $E_a = 10084.20$ (MWh). Obviously, the total PV modules area has a great influence on the annual energy, and therefore on the type of the rack configuration. In fact, the optimum β^* for each rack configuration is the same as the values of β for which the function $A_{TPV}(\beta)$ shows a maximum. However, there are 3 values of β in the $2V$ configuration to which the area $A_{TPV}(\beta)$ shows the same maximum value. These values are: 20, 21 and 22 (°). In that case, the method allows to choose which of these values is the optimum one that maximizes the energy basing on the other factors that affect the energy (16) in addition to the effective area $A_{PVeff}(n, \beta, T)$; these factors are $\cos\theta_i$ and $\cos\beta$.

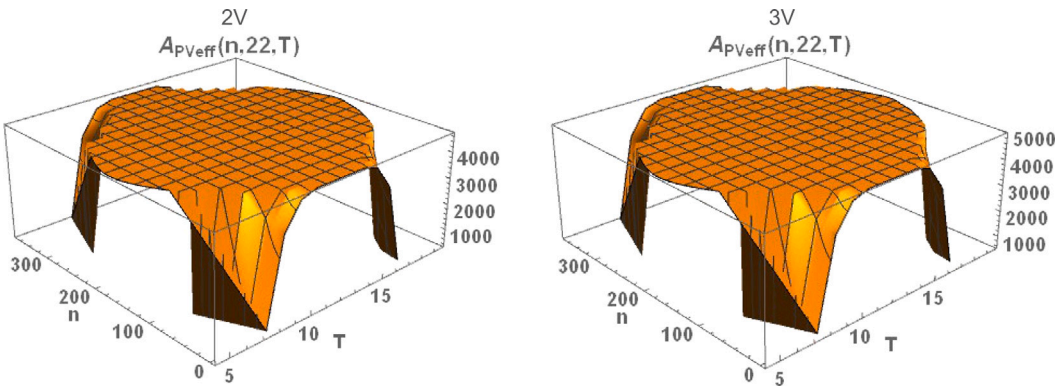

Fig. 9. Effective PV modules area, $A_{PVeff}(n, 22, T)$.

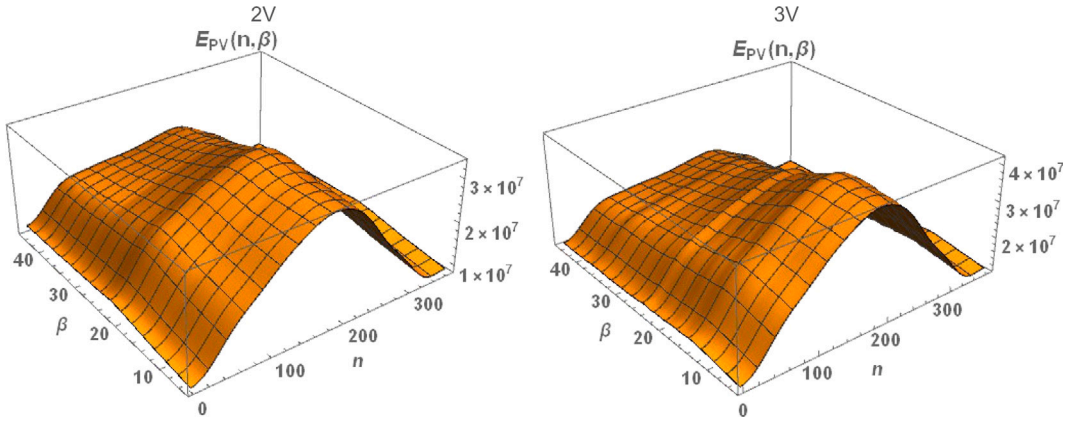

Fig. 10. Energy $E_{PV}(n, \beta)$.

Finally, the longitudinal spacing of maintenance e_l^m also has an important influence on the result. Until now this is the only parameter which has been given a fixed value.

In Fig. 11b the $e_l^m = 4.50$ (m) has been modified. An increase of e_l^m decreases the annual energy in both configurations and increases the value of the optimum tilt angle. These results are coherent because an increase of e_l^m decreases the number of rows of PV modules that can be installed in the North–South direction. Although it has to be pointed up that an increase of e_l^m, increases the value of the optimum tilt angle β. This result is explained again by the fact that the PV modules can be tilted without producing shading between the adjacent rows.

Eventually, Fig. 12 shows the optimal rack arrangements for each one of these configurations as well as the current implemented one in Sigena $2V^A$. It also proves the influence of the parameters W and L on the installation of PV modules. Given that the parameter W is 1.5 times bigger in the $2V$ configuration, in the East–West direction, more gaps in these configurations can be seen and that results in a smaller, total PV modules area. The gap between the PV modules in the North–South direction is affected by the longitudinal spacing for maintenance, and that causes the parameter L to have a bigger influence on the number of PV modules which can be installed. Therefore, given that the parameter L is bigger in the $3V$ configuration, it enhances the results. The lowest parameter W of the $3V$ configuration, enhances the packing in the East–West direction and it adapts better to the irregularities of the land.

In the $2V$ configurations with the same parameters W and L, the parameter that influences the total PV modules area is the longitudinal spacing for maintenance. For $\beta^* = 22$ (°) the parameter longitudinal spacing for maintenance has the minimum value of 4 (m), while for $\beta^* = 30$ (°) the longitudinal spacing for maintenance is bigger than 4 (m).

The algorithm output gives answers to the three posed questions: how many PV modules can be installed?, which is the tilt angle of the PV modules? and which is the right position for the PV modules?.

The Table 3 summarizes the results obtained with the proposed methodology for the three configurations that have been studied. The concept of energy gain is very useful to evaluate the different configurations. The energy gain is then calculated as the difference between the energy absorbed by the $2V^P$ configuration and the $2V^A$ configuration, as a % of energy: longitudinal spacing for maintenance $e_l^m = 4$ (m) and a transversal installation distance of $e_t = 0.30$ (m)

$$EG_1 = \frac{2V^P - 2V^A}{2V^A} \cdot 100 \tag{27}$$

The energy gain also can be calculated as the difference between the energy absorbed by the $3V^P$ configuration and that absorbed by the $2V^A$ configuration, as a % of energy:

$$EG_2 = \frac{3V^P - 2V^A}{2V^A} \cdot 100 \tag{28}$$

In relation to the annual energy, Table 2 suggests the following conclusions:

(i) A $3V^P$ configuration produces the most annual energy. This is due to the fact that this configuration has a lower W than the other

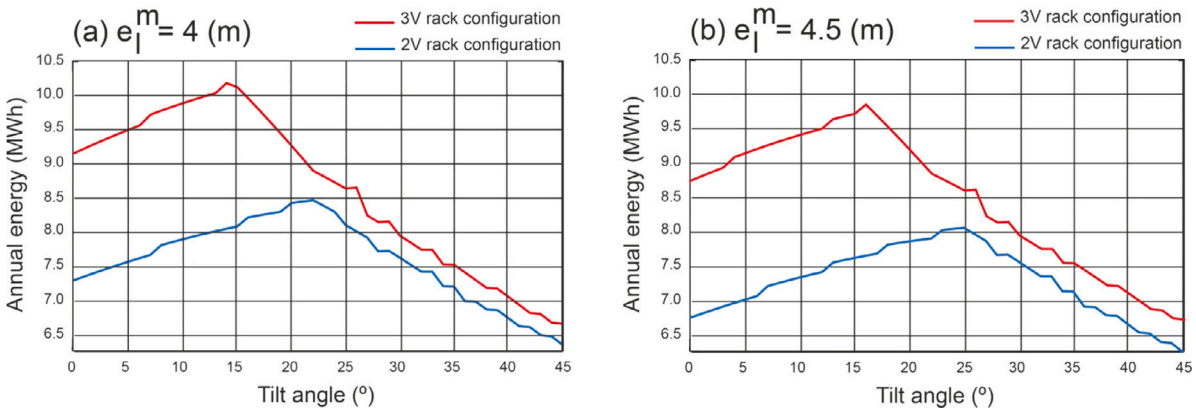

Fig. 11. Annual energy $E_a(\beta)$.

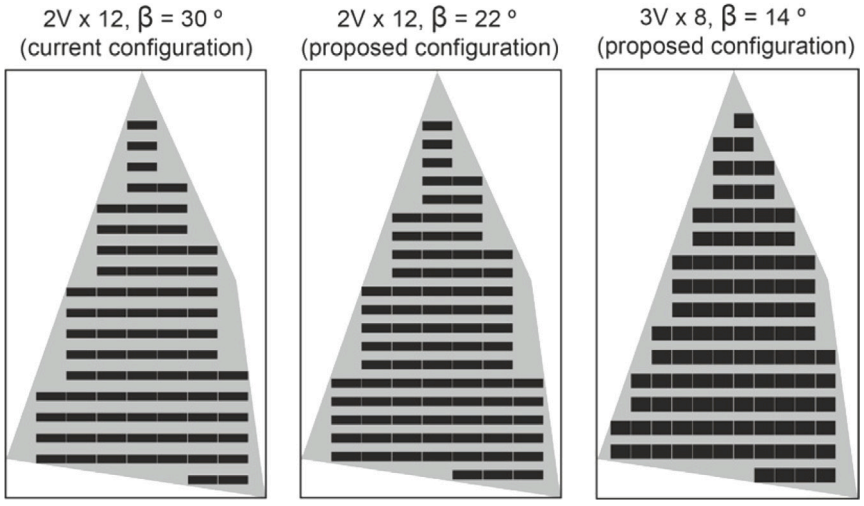

Fig. 12. Rows arrangement for the optimum distribution of PV modules.

Table 3
Results of Sigena I PV plant.

	2V × 12 ($2V^A$) actual config.	2V × 12 ($2V^P$) config. proposed	3V × 8 ($3V^P$) config. proposed
Input algorithm			
Area of $\overline{\mathbb{P}}$ (m^2)	11 402	11 402	11 402
Longitudinal maintenance distance (m)	4.00	4.00	4.00
Transversal installation distance (m)	0.30	0.30	0.30
Orientation	South	South	South
PV module model	JAM72S20 440–465/MR	JAM72S20 440–465/MR	JAM72S20 440–465/MR
Rack configuration	2V	2V	3V
Number of PV modules/rack	24	24	24
Output algorithm			
Number of total PV modules	1800	2016	2472
Number of rack	75	84	103
Tilt angle (°)	30	22	14
Longitudinal distance (m)	5.3621	4.01736	4.00
Annual solar irradiation (MWh)	7613.34	8436.96	10 084.20

three ones and, as a result of that, the algorithm packs more units in the East–West direction. Although this configuration has the greatest L, it produces a lower shading because it uses a low tilt angle Therefore, this configuration packs the most PV modules for the same surface.

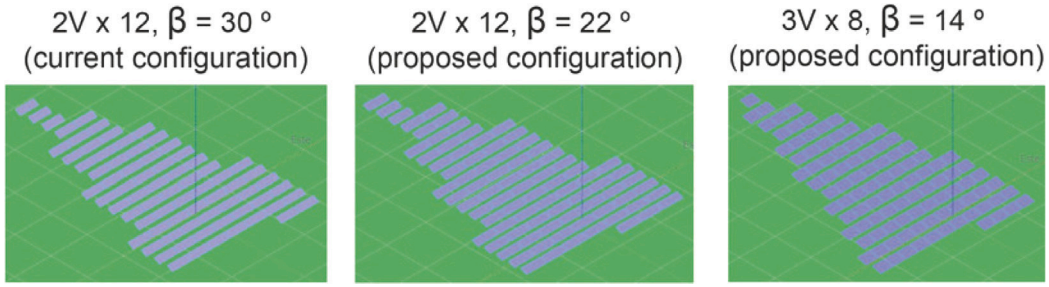

Fig. 13. Rows arrangement for the optimum distribution of PV modules (Screenshot from PVsyst).

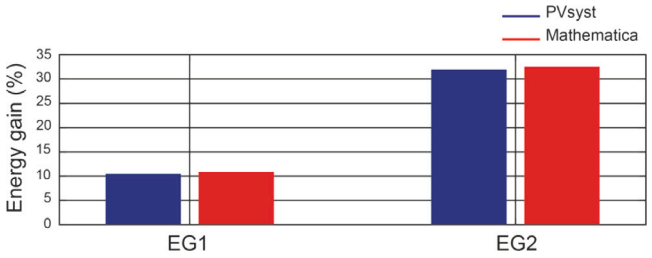

Fig. 14. Energy gain with Mathematica and PVsyst.

(ii) The current $2V^A$configuration gets the worst result. This is due to the fact that it uses a high tilt angle which is close to the site latitude and as a result of this, the produced shadows are very large and the rows of PV modules require more space in between them. This result, is supported by the work [27]. Therefore, the use of tilt angles whose values are close to the site latitude value impairs the whole PV plant results.

(iii) Both $2V^P$ and $2V^A$ configurations share the same parameters but the tilt angle. The $2V^P$ configuration gets better results than the $2V^A$ configuration because it uses a lower tilt angle and as a result of this it produces less shadows in between the PV modules.

(iv) The maximum EG_1 is 10.81% and the maximum EG_2 is 32.45%.

4.2. Verification by PVSyst software

In this work the PVsyst software [64] has been used to verify the energy gain across the different studied configurations: $2V^A$, $2V^P$, and $3V^P$. PVsyst software is a commercial software specialized in sizing and analysing PV systems. This software has been used by numerous authors for simulating photovoltaic systems [65,66]. Fig. 13 shows the design of the configurations with PVsyst.

Fig. 14 shows the graphical relative comparison between the Mathematica model and the PVsyst simulation for EG_1 and EG_2, which shows the practical equality between both models (0.56% at least, in relative terms).

4.3. Structural analysis of the mounting system

In the calculation of the ($2V^A$, $2V^P$ and $3V^P$) configurations, the typical environmental loads (wind and snow) as well as the weight of the structure itself, the weight of the PV modules, and combinations thereof have been analysed. The mounting angle of the $2V^A$ configuration is 30 (°), the one of the $2V^P$ configuration is 22 (°) and the one of the $3V^P$ configuration is 14 (°). In both cases 24 PV modules have been used. The model JAM72S20 440-465/MR manufactured by JA Solar, with a weight of 25 (Kg) and dimensions of 2120 × 1052 (mm) has been chosen for this study. Figs. 15 and 16 show the general views of these two configurations.

Table 4
Values for the wind action.

	$2V^A$ configuration	$2V^P$ configuration	$3V^P$ configuration
$q_{e\_pushing}$	1.015 (kN/m^2)	0.761 (kN/m^2)	0.62 (kN/m^2)
$q_{e\_suction}$	1.52 (kN/m^2)	1.269 (kN/m^2)	1.24 (kN/m^2)

The structural weight can be directly calculated by the software itself.

When calculating the load due to the weight of the PV modules, the following points have been taken into consideration:

(i) The weight of the PV module is 25 (kg).

(ii) The area of a PV module roughly is 2 (m^2).

According to the points (i) and (ii) and applying the Eq. (19), the load is of 0.125 (kN/m^2).

When calculating snow loading, the zone 2 and altitude of 235 (m) have been considered in the annex E of the code CTE DB-SE-AE [60]. Therefore, the maximum snow load is of −0.55 (kN/m^2).

When calculating wind actions, the following results have been obtained:

(i) As the installation is located in the zone B (See Table D.1 CTE DB SE-AE [60]), it results that q_b = 0.45 (kN/m^2) for both studied configurations.

(ii) The parameters to determine the exposure factor according to CTE DB SE-AE [60] are arranged in the Table D.2: Terrain of category II (Area with low vegetation such as grass and isolated obstacles (trees, buildings) with separations at least of 20 obstacle heights), z = 2 (m) for the $2V$ configuration and z = 2.4 (m) for the $3V$ configuration. Therefore, C_e = 1.88 (kN/m^2) for the $2V$ configuration and C_e = 1.97 (kN/m^2) for the $3V$ configuration.

(iii) The pressure coefficient can be calculated using the coefficients of the Eurocode 1, UNE-EN 1991-1-7: 2018 [56] for shed roofs at 30 (°), 22 (°) and 14 (°). The obtained values are: $C_{p\_pushing}$ = 1.2 by 30 (°), $C_{p\_suction}$ = 1.8 by 30 (°), $C_{p\_pushing}$ = 0.9 by 22 (°), $C_{p\_suction}$ = 1.5 by 22 (°), $C_{p\_pushing}$ = 0.7 by 14 (°), and $C_{p\_suction}$ = 1.4 by 14 (°).

(iv) In this case the probability factor is equal to 1.

The values of the wind action are shown in Table 4.

The AutoDesk Robot Structural Analysis [67] software has been used to calculate the structure. The program has several functions designed to simulate the behaviour of the structure under loads. As an example, Fig. 17 shows a simulation obtained with the AutoDesk Robot Structural Analysis software. The material and the geometrical properties of profiles obtained in the outputs of the AutoDesk Robot Structural Analysis software are summarized in Annex A while Annex B summarizes the dimensions of the structure.

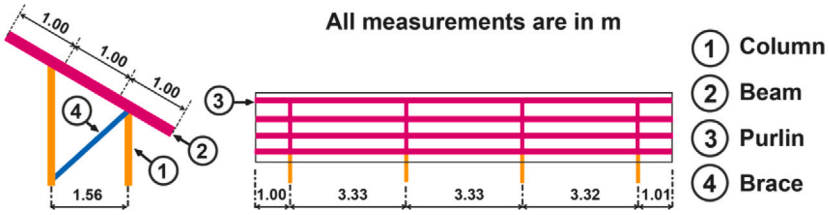

Fig. 15. Cross-section of the $2V^P$ configuration.

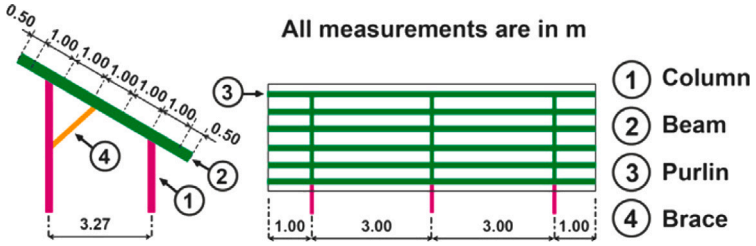

Fig. 16. Cross-section of the $3V^P$ configuration.

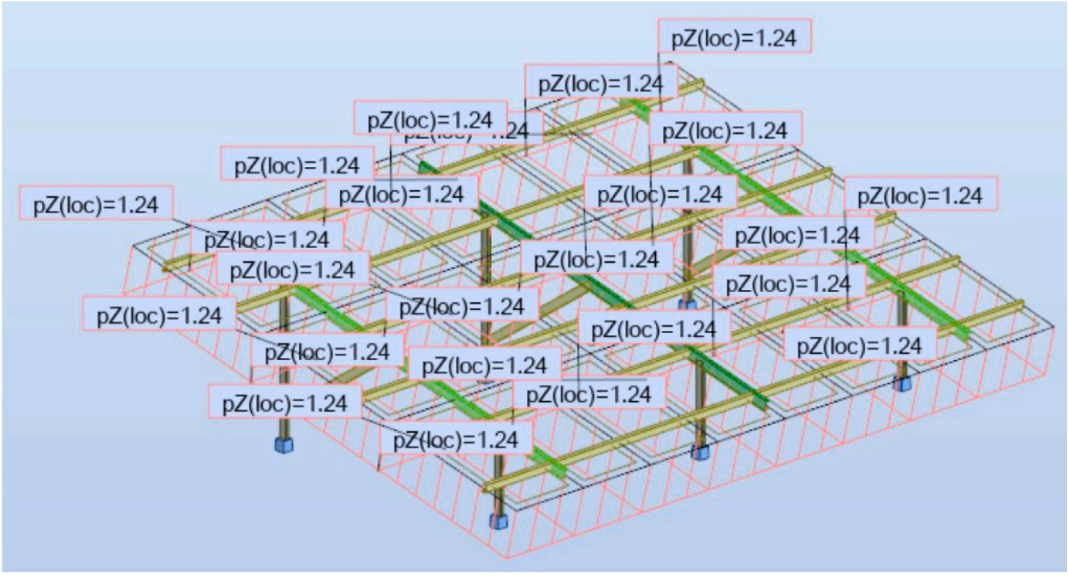

Fig. 17. Simulation obtained with the AutoDesk Robot Structural Analysis software.

4.4. Cost analysis of the mounting system

The weight of the elements (columns, beams, purlins, braces, driven piles) will be computed basing on the analysis of the structure section and the material properties.

All the costs of the structure necessary to calculate the cost of each configuration are listed in Annex C. All the cost are referred to date 26/05/2021. The calculation of the total cost of the mounting system is shown in Table 5. The $2V^A$ configuration is the more expensive one because it is the configuration with the biggest slope and therefore it has a greater wind load which requires an increase in the profiles of the purlins and the beams size.

Table 6 shows the costs of the parameters analysed in the configurations that have been studied. Obviously, the $3V^P$ configuration is the configuration that has the highest initial investment cost.

Table 5
Cost per configuration.

Configuration	Structure cost (€)	Other elements cost (€)	Total cost (€)
$2V^A$	693.22	74.64	767.86
$2V^P$	537.80	74.64	612.44
$3V^P$	504.97	72.37	579.34

The $LCOE$ of the rack configurations have been compared, taking as baseline the $3V^P$ configuration, by computing the ratio between the $LCOE$ of the $2V^A$ and the $2V^P$ configurations and this one (see Eq. (26)). This comparison shows that η_{LCOE} values are 1.10 and 1.05, respectively. Therefore the $2V^A$ configuration is the worst one in relation to the $LCOE$ value.

Table 6
Total cost.

Element	$2V^A$ configuration	$2V^P$ configuration	$3V^P$ configuration
N_{PV}	1800	2016	2472
C_{PV} (€) [68]	164.38	164.38	164.38
N_{MS}	75	84	103
C_{MS} (€)	767.86	612.44	579.34
$N_{PV}{\cdot}C_{PV}+N_{MS}{\cdot}C_{MS}$ (€)	353 473.72	382 834.98	466 046.74

5. Conclusions

A ground-mounted photovoltaic power plant comprises a high number of components: photovoltaic modules, mounting systems, inverters, power transformer, ... Therefore its optimization may have different approaches. This paper presents a methodology for estimating the optimal distribution of photovoltaic modules with a fixed tilt angle in a photovoltaic plant using a packing algorithm (in Mathematica™ software) that maximizes the amount of energy absorbed by the photovoltaic plant. A geospatial analysis of satellite imagery of plot areas has been used for the determination of the available land areas for the installation of photovoltaic plants. An open-source geographic information system software, *QGIS*, has been used. This software permits the conversion, visualization and analysis of geospatial data. Different rack configurations and tilt angles are incorporated in the study to account for the characteristics of the irregular shape of the land. The most used rack configurations in photovoltaic plants are the $2V \times 12$ configuration and the $3V \times 8$ configuration. Codes and standards have been used for the structural analysis of these rack configurations. For this purpose, the wind loads, the snow loads, the weight of the structure, the weight of the photovoltaic modules, and combinations thereof have be calculated. This analysis has been performed with AutoDesk Robot Structural Analysis software for different rack configurations. The main advantages of this methodology are:

(i) This methodology maximizes the amount of energy absorbed by the photovoltaic plant using a packing algorithm.

(ii) The packing algorithm calculates in an accurate way the shading between photovoltaic modules.

(iii) The algorithm output gives answers to the three posed questions: how many *PV* modules can be installed?, which is the tilt angle of the *PV* modules? and which is the right position for the *PV* modules?.

(iv) The methodology can be extended to any photovoltaic plant.

From a qualitative point of view, the following conclusions have been reached:

(i) The type of the rack configuration has a great influence on the amount of solar energy captured by a photovoltaic plant.

(ii) The parameters length of the rack configuration, width of the rack configuration, longitudinal spacing for maintenance and tilt angle of photovoltaic module have a great influence on the total photovoltaic modules area.

(iii) The gap between the photovoltaic modules in the North–South direction is affected by the longitudinal spacing for maintenance, and it gives rise to a bigger influence of the parameter length of the rack configuration on the number of photovoltaic modules that can be installed in that direction.

(iv) The gap between the photovoltaic modules in the North–South direction is affected by the longitudinal spacing for maintenance, and it gives rise to a smaller influence of the parameter length of the rack configuration on the number of photovoltaic modules that can be installed in that direction.

(v) The optimum tilt angle of the photovoltaic module to maximize the total photovoltaic modules area, will be got when the longitudinal distance has a similar value to that of the longitudinal spacing for maintenance.

(vi) The tilt angle that maximizes the total photovoltaic modules area has a great influence on the optimum tilt angle that maximizes the energy. In most of the cases both angles have the same value, but in some cases it is necessary to look at cosine of the incidence angle or at the model of Liu and Jordan for the diffuse and the ground reflected solar irradiation in order to distinguish which one is its optimum value.

(vii) The cost of the mounting system is deeply influenced by its tilt angle. The biggest the tilt angle is, the highest the cost of the mounting system becomes because the size of the profiles of the purlins and beams increases due to the wind loads.

The described methodology has been applied in Sigena I photovoltaic plant with a fixed tilt angle, $2V \times 12$ configuration with a tilt angle of 30 (°), located in Northeast of Spain (Villanueva de Sigena). From a quantitative point of view, the following conclusions have been reached:

(i) The configurations, $3V \times 8$ configuration with a tilt angle of 14 (°) and $2V \times 12$ configuration with a tilt angle of 22 (°), are the best options proposed by the packing algorithm.

(ii) The $3V \times 8$ configuration with a tilt angle of 14 (°) is the best option in relation to the total energy captured by the photovoltaic plant, due to the lower width of the rack configuration and its lower tilt angle, which allows more mounting systems to be packed. The $3V \times 8$ configuration increases the amount of energy captured by up to 32.45% in relation to the current of Sigena I photovoltaic plant and it also increases the amount of energy captured by up to 19.52% in relation to the $2V \times 12$ configuration with a tilt angle of 22 (°).

(iii) The current $2V \times 12$ configuration (30 (°)) absorbs 10.81% less energy and it is 25.37% more expensive than the proposed $2V \times 12$ configuration (22 (°)).

(iv) The $3V \times 8$ configuration with a tilt angle of 14 (°) is the one which has the lowest cost for the same number of photovoltaic modules. The $2V \times 12$ configuration with a tilt angle of 30 (°) increases the cost by up to 32.4% in relation to a $3V \times 8$ configuration with a tilt angle of 14 (°).

(v) The $2V \times 12$ configuration with a tilt angle of 30 (°) has the worst *LCOE* value. The *LCOE* efficiency of the $3V \times 8$ configuration is better than those of the $2V \times 12$ configuration with a tilt angle of 30 (°) and the $2V \times 12$ configuration with a tilt angle of 22 (°), whose efficiencies are respectively 1.10 and 1.05.

The methodology proposed can serve to make the optimal decisions in the choice of rack configurations of photovoltaic plants, yielding significant benefits from the point of view of total energy absorption and budget optimization. There are many *PV* system designers who would benefit from studies on this issue. A future work will consist of applying this methodology in different parts of the world to analyse the influence of the latitude of the location. Another possible extension of the work, certainly more ambitious, would be the application of the method to bifacial modules.

CRediT authorship contribution statement

A. Barbón: Conceptualization, Methodology. **C. Bayón-Cueli:** Software, Methodology, Writing – original draft. **L. Bayón:** Conceptualization, Methodology. **V. Carreira-Fontao:** Software, Conceptualization, Methodology.

Declaration of competing interest

The authors declare that they have no known competing financial interests or personal relationships that could have appeared to influence the work reported in this paper.

Acknowledgments

We wish to thank Gonvarri Solar Steel [16] for his contribution in this paper.

Table 7
Material and geometrical properties of profiles used in $2V^A$ configuration.

Element	Designation	Size (mm)	Thickness (mm)	Material	Weight/unit (kg/m)
Rear column	C100 × 50 × 20 × 3	C100 × 50 × 20	3	S 280GD Z275	5.652
Front column	C100 × 50 × 20 × 3	C100 × 50 × 20	3	S 280GD Z275	5.652
Driven pile	C100 × 50 × 20 × 3	C100 × 50 × 20	3	S 280GD Z275	5.652
Beam	C150 × 50 × 20 × 2	C150 × 50 × 20	2	S 280GD Z275	4.55
Purlin	C125 × 50 × 20 × 2	C125 × 50 × 20	2	S 280GD Z275	4.16
Brace	C100 × 50 × 20 × 1.5	C100 × 50 × 20	1.5	S 280GD Z275	2.826

Table 8
Material and geometrical properties of profiles used in $2V^P$ configuration.

Element	Designation	Size (mm)	Thickness (mm)	Material	Weight/unit (kg/m)
Rear column	C100 × 50 × 20 × 3	C100 × 50 × 20	3	S 280GD Z275	5.652
Front column	C100 × 50 × 20 × 3	C100 × 50 × 20	3	S 280GD Z275	5.652
Driven pile	C100 × 50 × 20 × 3	C100 × 50 × 20	3	S 280GD Z275	5.652
Beam	C125 × 50 × 20 × 2	C125 × 50 × 20	2	S 280GD Z275	4.16
Purlin	C100 × 50 × 20 × 2	C100 × 50 × 20	2	S 280GD Z275	3.76
Brace	C100 × 50 × 20 × 1.5	C100 × 50 × 20	1.5	S 280GD Z275	2.826

Table 9
Material and geometrical properties of profiles used in $3V^P$ configuration.

Element	Designation	Size (mm)	Thickness (mm)	Material	Weight/unit (kg/m)
Rear column	C100 × 50 × 20 × 3	C100 × 50 × 20	3	S 280GD Z275	5.652
Front column	C100 × 50 × 20 × 3	C100 × 50 × 20	3	S 280GD Z275	5.652
Driven pile	C100 × 50 × 20 × 3	C100 × 50 × 20	3	S 280GD Z275	5.652
Central beam	C125 × 50 × 20 × 2	C125 × 50 × 20	2	S 280GD Z275	4.16
Beam	C100 × 50 × 20 × 2	C100 × 50 × 20	2	S 280GD Z275	3.76
Purlin	C100 × 50 × 20 × 1.5	C100 × 50 × 20	1.5	S 280GD Z275	2.826
Brace	C100 × 50 × 20 × 1.5	C100 × 50 × 20	1.5	S 280GD Z275	2.826

Table 10
Dimensions of the structure with a $2V^A$ configuration.

Element	Designation	Units	Length (mm)
Rear column	C 100 × 50 × 20 × 3	4	2340
Front column	C 100 × 50 × 20 × 3	4	1640
Driven pile	C 100 × 50 × 20 × 3	8	1500
Beam	C 150 × 50 × 20 × 2	4	3000
Purlin	C 125 × 50 × 20 × 2	4	6000
Purlin	C 125 × 50 × 20 × 2	4	6000
Brace	C100 × 50 × 20 × 1.5	4	1300

Table 11
Dimensions of the structure with a $2V^P$ configuration.

Element	Designation	Units	Length (mm)
Rear column	C 100 × 50 × 20 × 3	4	1760
Front column	C 100 × 50 × 20 × 3	4	1237
Driven pile	C 100 × 50 × 20 × 3	8	1500
Beam	C 125 × 50 × 20 × 2	4	3000
Purlin	C100 × 50 × 20 × 2	4	6000
Purlin	C100 × 50 × 20 × 2	4	6000
Brace	C100 × 50 × 20 × 1.5	4	1300

Annex A. Material and geometrical properties of the profiles used

The material and geometrical properties of profiles obtained in the outputs of the AutoDesk Robot Structural Analysis software are summarized in Tables 7–9. In all these cases the surface treatment is Hot-Dip Galvanizing. Weight will be expressed per linear metre.

Annex B. Dimensions of the structure

The dimensions and number of the elements used are summarized in Tables 10–12.
They show that the driven piles are longer in the $3V^P$configuration, because it has less driven piles.

Annex C. Costs of the structure

The cost of the elements of the structure of the $2V^A$, $2V^P$ and $3V^P$ configurations are listed in Tables 13–15, respectively. All the cost are referred to date 26/05/2021.

The other components of the mounting system have also to be taken into account. There are: screws, washers, nuts, clamps and end clamps. The cost of the other $2V$ configuration elements and $3V$ configuration elements are listed in Table 16. All the cost are referred to date 26/05/2021.

Table 12
Dimensions of the structure with a $3V^P$ configuration.

Element	Designation	Units	Length (mm)
Rear column	C 100 × 50 × 20 × 3	3	1780
Front column	C 100 × 50 × 20 × 3	3	970
Driven pile	C 100 × 50 × 20 × 3	6	2300
Central beam	C 125 × 50 × 20 × 2	1	5410
Beam	C 100 × 50 × 20 × 2	2	5410
Purlin	C100 × 50 × 20 × 1.5	6	4000
Purlin	C100 × 50 × 20 × 1.5	6	4000
Brace	C100 × 50 × 20 × 1.5	3	1930

Table 13
Costs of the structure of the $2V^A$ configuration.

Element	Designation	Units	Length (mm)	Weight/unit (kg/m)	Total weight (kg)	Cost/kg* (€/kg)
Rear column	C 100 × 50 × 20 × 3	4	2340	5.652	39.79	1.44
Front column	C 100 × 50 × 20 × 3	4	1640	5.652	27.97	1.44
Driven pile	C 100 × 50 × 20 × 3	8	1500	5.652	67.82	1.44
Beam	C 150 × 50 × 20 × 2	4	3000	4.553	54.636	2.8
Purlin	C125 × 50 × 20 × 2	4	6000	4.160	99.84	1.45
Purlin	C125 × 50 × 20 × 2	4	6000	4.160	99.84	1.45
Brace	C100 × 50 × 20 × 1.5	4	1300	2.826	14.69	1.56

Table 14
Costs of the structure of the $2V^P$ configuration.

Element	Designation	Units	Length (mm)	Weight/unit (kg/m)	Total weight (kg)	Cost/kg* (€/kg)
Rear column	C 100 × 50 × 20 × 3	4	1760	5.652	39.79	1.44
Front column	C 100 × 50 × 20 × 3	4	1237	5.652	27.97	1.44
Driven pile	C 100 × 50 × 20 × 3	8	1500	5.652	67.82	1.44
Beam	C 125 × 50 × 20 × 2	4	3000	4.16	49.92	1.45
Purlin	C100 × 50 × 20 × 2	4	6000	3.76	90.24	1.37
Purlin	C100 × 50 × 20 × 2	4	6000	3.76	90.24	1.37
Brace	C100 × 50 × 20 × 1.5	4	1300	2.826	14.69	1.56

Table 15
Costs of the structure of the $3V^P$ configuration.

Element	Designation	Units	Length (mm)	Weight/unit (kg/m)	Total weight (kg)	Cost/kg* (€/kg)
Rear column	C 100 × 50 × 20 × 3	3	1780	5.652	30.18	1.44
Front column	C 100 × 50 × 20 × 3	3	970	5.652	16.447	1.44
Driven pile	C 100 × 50 × 20 × 3	6	2300	5.652	77.99	1.44
Central beam	C 125 × 50 × 20 × 2	1	5410	4.16	22.50	1.45
Beam	C 100 × 50 × 20 × 2	2	5410	3.76	40.68	1.37
Purlin	C100 × 50 × 20 × 1.5	6	4000	2.826	67.824	1.56
Purlin	C100 × 50 × 20 × 1.5	6	4000	2.826	67.824	1.56
Brace	C100 × 50 × 20 × 1.5	3	1930	2.826	16.36	1.56

Table 16
Costs of the other elements.

Element	Standard	Material	Surface treatment	Units for $2V^A - 2V^P$	Units for $3V^P$	Cost/un* (€/un)
Screw M12 × 30	DIN 933	Class 8.8	Hot-Dip Galv.	33	31	0.2852
Wide flat washer M12	DIN 9021	Class 8.8	Hot-Dip Galv.	66	62	0.3244
Grower washer M12	DIN 127	Class 8.8	Hot-Dip Galv.	33	31	0.0456
Nut M12	DIN 934	Class 8.8	Hot-Dip Galv.	33	31	0.076
Screw M8 × 50	DIN 933	Class 8.8	Stainless	45	43	0.19
Washer M8	DIN 9021	Class 8.8	Stainless	45	43	0.0434
Nut M8	DIN 934	Class 8.8	Stainless	45	43	0.0411
Screw M8 × 40	DIN 933	Class 8.8	Stainless	9	13	0.17
Washer M8	DIN 9021	Class 8.8	Stainless	9	13	0.0434
Nut M8	DIN 934	Class 8.8	Stainless	9	13	0.0411
Clamp	DIN 933	Aluminium		45	43	0.39
End clamp	DIN 933	Aluminium		9	13	0.33
Sheet for brace		S280GD Z275	Hot-Dip Galv.	4	3	1.16

References

[1] United Nations (UNFCC). Report of the conference of the parties onits twenty-first session, Paris, November to December 2015. 2016, Available from: http://unfccc.int/resource/docs/2015/cop21/eng/10a01.pdf [Accessed 20.08.16].

[2] EU. On the promotion of the use of energy from renewable sources. Directive 2016/0382/EC, 2016.

[3] Bp statistical review of world energy. 2020.

[4] IRENA. Future of Solar Photovoltaic: Deployment, Investment, Technology, Grid Integration and Socio-Economic Aspects. International Renewable Energy Agency; 2019, Available from https://irena.org/-/media/Files/IRENA/Agency/Publication/2019/Nov/IRENA_Future_of_Solar_PV_2019.pdf [Accessed on 23 December 2020].

[5] Talavera DL, Muñoz Cerón Emilio, Ferrer-Rodríguez JP, Pérez-Higueras PJ. Assessment of cost-competitiveness and profitability of fixed and tracking photovoltaic systems: The case of five specific sites. Renew Energy 2019;134:902–13.

[6] Mortensen J. Factors associated with photovoltaic system costs. Golden CO: National REnewable Energy Laboratory; 2001.

[7] Cabrera-Tobar A, Bullich-Massagué E, Aragüés-Peñalba M, Gomis-Bellmunt O. Topologies for large scale photovoltaic power plants. Renew Sustain Energy Rev 2016;59:309–19.

[8] Denholm P, Margolis RM. Land-use requirements and the per-capita solar footprint for photovoltaic generation in the United States. Energy Policy 2008;36:3531–43.

[9] Zidane TEK, Adzman MRB, Tajuddin MFN, Zalia SM, Durusu A. Optimal configuration of photovoltaic power plant using grey wolf optimizer: A comparative analysis considering CdTe and c-Si PV modules. Sol Energy 2019;188:247–57.

[10] Bakhshi-Jafarabadi R, Sadeh J, Soheili A. Global optimum economic designing of grid-connected photovoltaic systems with multiple inverters using binary linear programming. Sol Energy 2019;183:842–50.

[11] Simola A, Kosonen A, Ahonen T, Ahola J, Korhonen M, Hannula T. Optimal dimensioning of a solar PV plant with measured electrical load curves in Finland. Sol Energy 2018;170:113–23.

[12] Şenol M, Abbasoğlu S, Kükrer O, Babatunde AA. A guide in installing large-scale PV power plant for self consumption mechanism. Sol Energy 2016;132:518–37.

[13] Sulaiman SI, Rahman TKA, Musirin I, Shaari S, Sopian K. An intelligent method for sizing optimization in grid-connected photovoltaic system. Sol Energy 2012;86:2067–82.

[14] Fernández-Infantes A, Contreras J, Bernal-Agustín JL. Design of grid connected PV systems considering electrical, economical and environmental aspects: A practical case. Renew Energy 2006;31:2042–62.

[15] Barbón A, Fortuny Ayuso P, Bayón L, Silva CA. A comparative study between racking systems for photovoltaic power systems. Renew Energy 2021;180:424–37.

[16] Gonvarri solar steel. 2021, Available from: https://www.gsolarsteel.com/ [Accessed on: 23 June 2021].

[17] Fthenakis V, Kim HC. Land use and electricity generation: A life-cycle analysis. Renew Sustain Energy Rev 2009;13:1465–74.

[18] Ong S, Campbell C, Denholm P, Margolis R, Heath G. Land use requirements for solar power plants in the united states. Technical report NREL/TP-6A20-56290, National Renewable Energy Laboratory; 2013, p. 39.

[19] Martín-Chivelet N. Photovoltaic potential and land-use estimation methodology. Energy 2016;94:233–42.

[20] Narvarte L, Lorenzo E. Tracking and ground cover ratio. Prog Photovolt: Res Appl 2008;16:703–14.

[21] Hermann S, Miketa A, Fichaux N. Estimating the renewable energy potential in africa. IRENA-KTH working paper, Abu Dhabi: International Renewable Energy Agency; 2014.

[22] Verso A, Martín A, Amador J, Domínguez J. Gis-based method to evaluate the photovoltaic potential in the urban environments: The particular case of miraflores de la sierra. Sol Energy 2015;117:236–45.

[23] Yang Q, Huang T, Wang S, Li J, Dai S, Wright S, Wang Y, Peng H. A GIS-based high spatial resolution assessment of large-scale PV generation potential in China. Appl Energy 2019;247(2019):254–69.

[24] Lindberg O, Birging A, Widén J, Lingfors D. Pv park site selection for utility-scale solar guides combining GIS and power flow analysis: A case study on a Swedish municipality. Appl Energy 2021;282:116086.

[25] Zhang Y, Ren J, Pu Y, Wang P. Solar energy potential assessment: a framework to integrate geographic, technological, and economic indices for a potential analysis. Renew Energy 2020;149:577–86.

[26] Barbón A, Barbón N, Bayón L, Sánchez-Rodríguez JA. Optimization of the distribution of small scale linear fresnel reflectors on roofs of urban buildings. Appl Math Model 2018;59:233–50.

[27] Barbón A, Bayón-Cueli C, Bayón L, Rodríguez-Suanzes C. Analysis of the tilt and azimuth angles of photovoltaic systems in non-ideal positions for urban applications. Appl Energy 2022;305:117802, 1-14.

[28] Doorga JRS, Rughooputh SDDV, Boojhawon R. Multi-criteria GIS-based modelling technique for identifying potential solar farm sites: A case study in mauritius. Renew Energy 2019;133:1201–19.

[29] Yushchenko A, Bono A, Chatenoux B, Patel MK, Ray N. Gis-based assessment of photovoltaic (PV) and concentrated solar power (CSP) generation potential in West Africa. Renew Sustain Energy Rev 2018;81:2088–103.

[30] Alami Merrouni A, Elwali Elalaoui F, Mezrhab A, Mezrhab A, Ghennioui A. Large scale PV sites selection by combining GIS and analytical hierarchy process, case study: Eastern Morocco. Renew Energy 2018;119:863–73.

[31] IRENA. Unleashing the solar potential in ecowas: seeking areas of opportunity for grid-connected and decentralised pv applications. International Renewable Energy Agency; 2013.

[32] Giamalaki M, Tsoutsos T. Sustainable siting of solar power installations in mediterranean using a GIS/AHP approach. Renew Energy 2019;141:64–75.

[33] Saraswat SK, Digalwar AK, Yadav SS, Kumar G. MCDM And GIS based modelling technique for assessment of solar and wind farm locations in India. Renew Energy 2021;169:865–84.

[34] Zhang Y, Chen H, Du Y. Considerations of photovoltaic system structure design for effective lightning protection. IEEE Trans Electromagn Compat 2020;62:1333–41.

[35] Chinchilla M, Santos-Martín D, Carpintero-Rentería M, Lemon S. Worldwide annual optimum tilt angle model for solar collectors and photovoltaic systems in the absence of site meteorological data. Appl Energy 2021;281:116056.

[36] Antonanzas-Torres F, Urraca R, J. Polo J, Perpiñán-Lamigueiro O, Escobar R. Clear sky solar irradiance models: A review of seventy models. Renew Sustain Energy Rev 2019;107:374–87.

[37] Salazar G, Gueymard C, Galdino JBezerra, Vilela OCastro. Solar irradiance time series derived from high-quality measurements, satellite-based models, and reanalyses at a near-equatorial site in Brazil. Renew Sustain Energy Rev 2020;117:109478.

[38] Fan J, Chen B, Wu L, Zhang F, Lu X. Evaluation and development of temperature-based empirical models for estimating daily global solar radiation in humid regions. Energy 2018;144:903–14.

[39] Barbón A, Ayuso PFortuny, Bayón L, Fernández-Rubiera JA. Predicting beam and diffuse horizontal irradiance using Fourier expansions. Renew Energy 2020;154:46–57.

[40] Hottel HC. A simple model for estimating the transmittance of direct solar radiation through clear atmosphere. Sol Energy 1976;18:129–34.

[41] Liu BYH, Jordan RC. The interrelationship and characteristic distribution of direct, diffuse and total solar radiation. Sol Energy 1960;4(3):1–19.

[42] PVGIS. Joint Research Centre JRC, 2020. Available from: http://re.jrc.ec.europa.eu/pvg_tools/en/tools.html [Accessed on: 6 March 2021].

[43] WRDC. World radiation data centre. 2020, Available from: http://wrdc.mgo.rssi.ru/ [Accessed on: 6 March 2021].

[44] Duffie JA, Beckman WA. Solar engineering of thermal processes. John Wiley & Sons; 2013.

[45] Al-Khazzar A. The required land area for installing a photovoltaic power plant. Iran J Energy Environ 2017;8:11–7.

[46] Sebbah B, Yazidi Alaoui O, Wahbi M, Maâtouk M, Ben Achhab N. QGIS-Landsat indices plugin (Q-LIP): Tool for environmental indices computing using landsat data. Environ Model Softw 2021;137:104972.

[47] Park S, Nielsen A, Bailey RT, Trolle D, Bieger K. A QGIS-based graphical user interface for application and evaluation of SWAT-MODFLOW models. Environ Model Softw 2019;111:493–7.

[48] NGIC. National geographic information centre of the government of Spain. 2021, Available from: http://centrodedescargas.cnig.es/CentroDescargas/ [Accessed on: 23 June 2021].

[49] Wolfram mathematica software. 2022, Available from: https://www.wolfram.com/mathematica/ [Accessed on: 23 January 2022].

[50] IDAE. Technical conditions for pv installations connected to the grid [in Spanish]. Spanish government technical report, Available from: http://www.idae.es (Accessed 1 October 2021).

[51] Makhdoomi S, Askarzadeh A. Impact of solar tracker and energy storage system on sizing of hybrid energy systems: A comparison between diesel/PV/PHS and diesel/PV/FC. Energy 2021;231:120920.

[52] Mamun MAA, Islam MM, Hasanuzzaman M, Selvaraj J. Effect of tilt angle on the performance and electrical parameters of a PV module: Comparative indoor and outdoor experimental investigation. Energy Built Environ 2021. xxx:xxx.

[53] Conceiçao R, Silva HG, Fialho L, Lopes FM, Collares-Pereira M. Pv system design with the effect of soiling on the optimum tilt angle. Renew Energy 2019;133:787–96.

[54] Liu BYH, Jordan RC. The long-term average performance of flat-plate solar energy collectors. Sol Energy 1963;7:53–74.

[55] UNE-EN 1990. Basis of structural design. AENOR; 2019.

[56] UNE-EN 1991-1-7. Actions on structures. AENOR; 2018.

[57] UNE-EN 1993-1-9:2013. Design of steel structures. AENOR; 2013.

[58] UNE-EN ISO 1461:2010. Hot dip galvanized coatings on fabricated iron and steel articles. EANOR; 2010.

[59] UNE-EN ISO 14713-1:2017. Zinc coatings - guidelines and recommendations for the protection against corrosion of iron and steel in structures. AENOR; 2017.

[60] Spanish technical building code royal decree 314/2006. 2006.

[61] Zidane TEKhalil, Adzman MRBin, Tajuddin MFNaim, Zali SMat, Durusu A. Optimal configuration of photovoltaic power plant using grey wolf optimizer: A comparative analysis considering CdTe and c-Si PV modules. Sol Energy 2019;188:247–57.

[62] NREL. Best practices for operation and maintenance of photovoltaic and energy storage systems. 3rd ed.. Golden, CO: National Renewable Energy Laboratory; 2018, Available from https://www.nrel.gov/docs/fy19osti/73822.pdf [Accessed on: 23 June 2021].

[63] Branker K, Pathak MJM, Pearce JM. A review of solar photovoltaic levelized cost of electricity. Renew Sustain Energy Rev 2011;15:4470–82.

[64] PVsyst. Synthetic hourly irradiance. 2021, Available from: http://files.pvsyst.com/help/models_meteo_synthetic_generation_irradiance.htm [Accessed on: 23 June 2021].

[65] Yang Y, Campana PElia, .Stridh B, Yan J. Potential analysis of roof-mounted solar photovoltaics in Sweden. Appl Energy 2020;279:115786.

[66] Dey D, B. Subudhi. Design, simulation and economic evaluation of 90kWgrid connected photovoltaic system. Energy Rep 2020;6:1778–87.

[67] Ken M. Autodesk robot structural analysis professional 2016 - essentials. Marsh API; 2016.

[68] Autosolar. Technical data. 2021, Available from: https://autosolar.es/ [Accessed on: 23 June 2022].